

Optimal Defender Strategies for CAGE-2 using Causal Modeling and Tree Search

Kim Hammar [†], Neil Dhir [‡], and Rolf Stadler[†]

[†] KTH Royal Institute of Technology, Sweden

[‡] Siemens Technology, USA

Email: {kimham, stadler}@kth.se, neil.dhir@siemens.com

October 23, 2024

Abstract—The CAGE-2 challenge is considered a standard benchmark to compare methods for autonomous cyber defense. Current state-of-the-art methods evaluated against this benchmark are based on model-free (offline) reinforcement learning, which does not provide provably optimal defender strategies. We address this limitation and present a formal (causal) model of CAGE-2 together with a method that produces a provably optimal defender strategy, which we call Causal Partially Observable Monte-Carlo Planning (C-POMCP). It has two key properties. First, it incorporates the causal structure of the target system, i.e., the causal relationships among the system variables. This structure allows for a significant reduction of the search space of defender strategies. Second, it is an online method that updates the defender strategy at each time step via tree search. Evaluations against the CAGE-2 benchmark show that C-POMCP achieves state-of-the-art performance with respect to effectiveness and is two orders of magnitude more efficient in computing time than the closest competitor method.

Index Terms—cybersecurity, network security, causal inference, SCM, APT, CAGE-2, POMDP, intrusion response.

I. INTRODUCTION

Domain experts have traditionally defined and updated an organization’s security strategy. Though this approach can offer basic security for an organization’s IT infrastructure, a growing concern is that infrastructure update cycles become shorter and attacks increase in sophistication. To address this challenge, significant research efforts to automate the process of obtaining effective security strategies have started [1]–[3]. A driving factor behind this research is the development of evaluation benchmarks, which allow researchers to compare the performance of different methods. Presently, the most popular benchmark is the Cyber Autonomy Gym for Experimentation 2 (CAGE-2) [4], which involves defending a networked system against an Advanced Persistent Threat (APT), see Fig. 1.

At the time of writing, more than 30 methods have been evaluated against CAGE-2 [4]. Detailed descriptions of some methods can be found in [5]–[21]. While good results have been obtained, key aspects remain unexplored. For example, current methods are narrowly focused on *offline* reinforcement

DISTRIBUTION STATEMENT A (Approved for Public Release, Distribution Unlimited). This research is supported by the Defense Advanced Research Project Agency (DARPA) through the CASTLE program under Contract No. W912CG23C0029. The views, opinions, and/or findings expressed are those of the authors and should not be interpreted as representing the official views or policies of the Department of Defense or the U.S. Government.

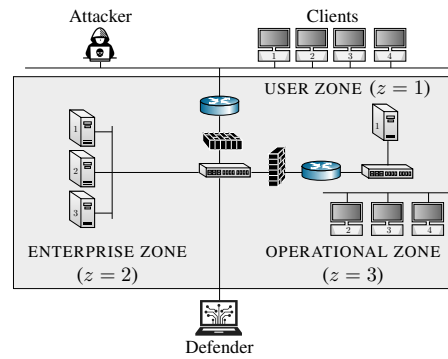


Fig. 1: The CAGE-2 scenario [4]: a defender aims to protect a networked system against an Advanced Persistent Threat (APT) caused by an attacker while maintaining services for clients; the system configuration is listed in Appendix D.

learning and require a lengthy training phase to obtain effective strategies. Further, these methods are *model-free* and do not provide provably optimal strategies. In addition, current methods provide limited ways to include domain expertise in the learning process, though attempts have been made with reward shaping [7].

In this paper, we address the above limitations and use the CAGE-2 scenario to illustrate and evaluate our solution method. First, we develop a formal (causal) model of CAGE-2, which allows us to define and prove the existence of an optimal defender strategy. This model is based on the source code of CAGE-2 and is formalized as a Structural Causal Model (SCM) [22, Def 7.1.1]. We prove that this SCM is equivalent to a specific Partially Observed Markov Decision Process (POMDP) [23, P.1]. Compared to the POMDP, our SCM offers a more expressive representation of the underlying causal structure, allowing us to understand the causal effects of defender strategies [22, Def. 3.2.1].

Second, we design an online method that produces a *provably optimal* defender strategy, which we call *Causal Partially Observable Monte-Carlo Planning* (C-POMCP). The method has two key properties: (1) it incorporates causal information of the target system in the form of a *causal graph* [22, Def. 2.2.1], which allows us to prune the search space of defender strategies; and (2) it is an *online* method that updates the defender strategy at each time step via *tree search*.

Our causal model represents one of many ways of formally

modeling CAGE-2. A key question is the level of abstraction at which CAGE-2 is modeled. The more detailed we construct the model, the closer it can capture the CAGE-2 implementation. However, this comes at the expense of higher computational complexity and lower generalization ability. When balancing this trade-off, we follow the principle that a model should be detailed enough so that a theoretically optimal defender strategy exhibits state-of-the-art performance in a practical implementation [4].

We evaluate C-POMCP against the CAGE-2 benchmark and show that it achieves state-of-the-art effectiveness while being two orders of magnitude more computationally efficient than the closest competitor method: CARDIFF-PPO [5]. The evaluation results also show that C-POMCP performs significantly better than its non-causal version: POMCP [24, Alg. 1]. While prior work has focused on offline methods that require hours of training, C-POMCP produces equally effective defender strategies through less than 15 seconds of online search.

Our contributions can be summarized as follows:

- We present a causal model of the CAGE-2 scenario (M1). This model allows us to define and prove the existence of optimal defender strategies (Thm. 1).
- We design C-POMCP, an online method that leverages the causal structure of the target system to efficiently find an optimal defender strategy (Alg. 1). C-POMCP includes a novel approach to leverage causal information for tree search, which may be of independent interest. The code is available at [25].
- We prove that C-POMCP converges to an optimal strategy with increasing search time (Thm. 4).
- We evaluate C-POMCP against the CAGE-2 benchmark. The results show that C-POMCP outperforms the current state-of-the-art methods in effectiveness and performs significantly better in computational efficiency [5].

II. RELATED WORK

Autonomous cyber defense is an active area of research that uses concepts and methods from various fields (see Fig. 2): reinforcement learning [3], [9], [11]–[13], [16]–[18], [20], [26]–[38], control theory [2], [39]–[46], causal inference [47]–[50], game theory [1], [51]–[61], rule-based systems [62]–[67], large language models [19], [21], [68], [69], evolutionary computation [70]–[75], and general optimization [76]–[80]. Several of these works use the CAGE-2 benchmark [4] for evaluating their methods, see for example [5]–[13], [16]–[21]. The best benchmark performance is achieved by those methods that are based on deep reinforcement learning, where the current state-of-the-art methods use Proximal Policy Optimization (PPO) [81, Alg. 1][5].

To our knowledge, no prior work has provided a formal model of CAGE-2, nor considered tree search for finding effective defender strategies. Moreover, the only prior works that use causal inference are [47]–[50]. This paper differs from them in two ways. First, the studies presented in [48]–[50] use causality for analyzing the effects of attacks and countermeasures but do not present methods for finding defender strategies. Second, the method for finding defender strategies

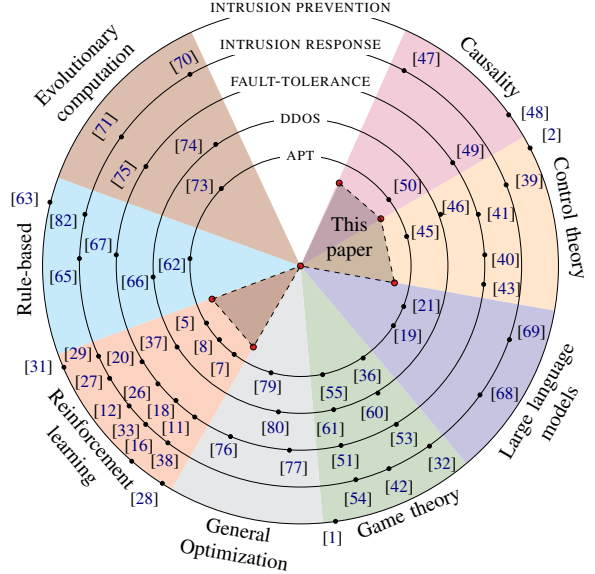


Fig. 2: Related work on autonomous cyber defense; this paper addresses APT defense using causality, control theory, and reinforcement learning.

in [47] uses Bayesian optimization and is *myopic*, i.e., it does not consider the future when selecting strategies. While this approach simplifies computations, the method is sub-optimal for most practical scenarios. By contrast, our method is non-myopic and produces optimal strategies (Thm. 4).

III. THE CAGE-2 SCENARIO

The CAGE-2 scenario involves defending a networked system against APTs [4]. The operator of the system, which we call the defender, takes measures to protect it against an attacker while providing services to a client population (see Fig. 1). The system is segmented into *zones* with *nodes* (servers and workstations) that run network services. Services are realized by *workflows* that are accessed by clients through a gateway, which is also open to the attacker. The detailed system configuration can be found in Appendix D.

The attacker aims to intrude on the system and disrupt service for clients. To achieve this goal, it can take five actions: scan the network to discover nodes; exploit a vulnerability to compromise a node; perform a brute force attack to obtain login credentials to a node; escalate privileges on a compromised node to gain root access; and disrupt the service on a compromised node.

The defender monitors the system through log files and network statistics. It can make four types of *interventions* on a node to prevent, detect, and respond to attacks: analyze the node for a possible intrusion; start a decoy service on the node; remove malware from the node; and restore the node to a secure state, which temporarily disrupts its service. When deciding between these interventions, the defender balances two conflicting objectives: maximize service utility towards its clients and minimize the cost of attacks.

IV. CAUSAL INFERENCE PRELIMINARIES

This section covers notation and provides an overview of causal inference, which lays the foundation for the subsequent

Notation(s)	Description
$\mathcal{G}_S, \mathcal{G}_W$	System graph and workflow graph (§V-A)
$\mathcal{V}, \mathcal{E}, \mathcal{Z}$	Set of nodes and edges in \mathcal{G}_S , set of zones (§V-A)
$\mathbf{D}_t, \mathbf{I}_t, \mathbf{S}_t$	Decoy states, intrusion states, and service states (§V-A)
U, K, S	The unknown, known, and scanned intrusion states (Fig. 5)
C, R	The compromised and root intrusion states (Fig. 5)
\mathbf{A}_t, α_t	Attacker action and attacker action type (§V-B)
V_t, P_t, T_t	Vulnerability, privileges, and target of attacker action (§V-B)
S, E, P	Scan, exploit, and privilege escalation attacker actions (§V-B)
I, D	Impact and discover attacker actions (§V-B)
f_t, f_S, f_C	Causal functions for $I_{i,t}$ (5), $S_{i,t}$ (6), and C_t (8)
$Z_{i,t}, \mathbf{Z}_t$	Observation of node i and observations for all nodes (§V-C)
$f_{Z,i}, W_{i,t}, \mathbf{W}_t$	Causal function for $Z_{i,t}$ (7), noise variable, noise variables
$C_t, \mathcal{A}_t, \mathcal{D}_t$	Number of clients, arrivals, and departures (8)
$\hat{\mathbf{X}}_t, \hat{\mathbf{x}}_t, \mathcal{T}$	Intervention variables and values (§V-E), search operator (18)
$\text{do}(\hat{\mathbf{X}}_t = \hat{\mathbf{x}}_t)$	Intervention at time t (10)
$\text{do}(\hat{\mathbf{X}}_t^* = \mathbf{x}_t^*)$	Optimal intervention at time t
R_t, J	Defender reward at time t and defender objective (9)
f_R, f_J, f_D	Causal functions of R_t , J (9), and $D_{i,t}$
U, V	Exogenous and endogenous variables (M1)
X_t, N_t	Manipulative, non-manipulative variables (§V-F)
O_t, L_t, F_A	Observed and latent variables (§V-F), causal function of A_t (4)
Y_t, D	Target variables (§V-F) at time t , set of decoys (Appendix D)
\mathcal{M}, \mathbf{F}	SCM and causal functions (M1)
$\mathbf{o}_t, \mathcal{T}$	Observation (12) and time horizon (9)
H_t, h_t, γ	History and its realization (11), discount factor
$\pi_A, \pi_D \in \Pi$	Attacker and defender strategies (§V-B and §V-E)
π_D^*, \mathfrak{R}	Optimal defender strategy (Thm. 1), cumulative regret (20)
$q_t, \psi_{z_t}, \beta_{z_t}$	Parameters in the defender objective (9)
$\hat{\mathbf{b}}_t, \mathbf{P}_G^*$	Belief state (14), the set of POMIIS (Def. 3)
$\Sigma_t, \sigma, \mathcal{G}$	Markov state and its realization (Thm. 1), causal graph (Fig. 6)
M, s_T, c	Number of particles, search time, exploration parameter (17)

TABLE 1: Notation.

section, where we deduce a causal model of the CAGE-2 scenario.

Notation. Random variables are denoted by upper-case letters (e.g., X), their values by lower-case letters (e.g., x), and their domains by $\text{dom}(\cdot)$. $X \perp\!\!\!\perp Y$ means that X and Y are independent. P is a probability measure. (Since we focus on countable sample spaces, the construction of the underlying probability space is standard.) The expectation of f with respect to X is written as $\mathbb{E}_X[f]$, and $x \sim f$ means that x is sampled from f . (As the sample spaces are countable, no question of the existence of $\mathbb{E}_X[f]$ will arise.) If f includes many random variables that depend on π , we simply write $\mathbb{E}_\pi[f]$. We use $P(x)$ as a shorthand for $P(X = x)$. Random vectors (or sets) and their values are written in bold upper-case and lower-case letters, respectively (e.g., \mathbf{X} and \mathbf{x}). A (column) vector is written as (x_1, x_2, \dots) and a 1-dimensional vector as $(x_1,)$. $\mathbb{1}$ is the indicator function. $\text{pa}(X)_G, \text{ch}(X)_G, \text{an}(X)_G$ and $\text{de}(X)_G$ denote parents, children, ancestors, and descendants of node X in a graph \mathcal{G} . $\mathcal{G}[\mathbf{V}]$ denotes the subgraph obtained by restricting \mathcal{G} to the nodes in \mathbf{V} . Further notation is listed in Table 1.

A. Structural Causal Models

A Structural Causal Model (SCM) is defined as

$$\mathcal{M} \triangleq \langle \mathbf{U}, \mathbf{V}, \mathbf{F}, P(\mathbf{U}) \rangle, \quad (1)$$

where \mathbf{U} is a set of *exogenous* random variables and \mathbf{V} is a set of *endogenous* random variables [22, Def 7.1.1]. Within $\mathbf{V} \cup \mathbf{U}$ we distinguish between five subsets that may overlap: the set of *manipulative* variables \mathbf{X} ; *non-manipulative* \mathbf{N} ; *observed* \mathbf{O} ; *latent* \mathbf{L} ; and *targets* \mathbf{Y} . (SCMs with latent variables are called “partially observable” [83, Def. 1].)

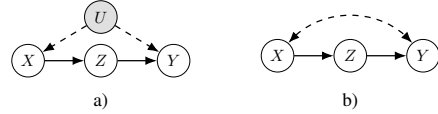


Fig. 3: Causal graphs [22, Def. 2.2.1]; circles represent variables in an SCM (1); solid arrows represent causal relations, and dashed edges represent effects caused by latent variables; latent variables can either be represented with shaded circles or with bidirected dashed edges, i.e., the graphs in a) and b) represent the same causal structure.

An SCM induces a *causal graph* \mathcal{G} [22, Def. 2.2.1], where nodes correspond to $\mathbf{V} \cup \mathbf{U}$ and edges represent (causal) functions $\mathbf{F} \triangleq \{f_i\}_{V_i \in \mathbf{V}}$. A function f_i is a mapping from the domains of a subset $\mathbf{K} \subseteq (\mathbf{U} \cup \text{pa}(V_i)_G)$ to the domain of V_i , which is represented graphically by directed edges from the nodes in \mathbf{K} to V_i (see Fig. 3). If each function is independent of time, the SCM is said to be *stationary*.

Causal graphs with latent variables can be drawn in two ways (cf. Fig. 3.a and Fig. 3.b). One option is to include the latent variables in the graph (Fig. 3.a). Another option is to represent the latent variables with bidirected edges, where a bidirected edge between two observed variables means that they share an *unobserved confounder* [22, Def. 6.2.1], i.e., a latent variable that influences both of them (Fig. 3.b).

We say that $P(\mathbf{V})$ is Markov relative to \mathcal{G} if it admits the following factorization [22, Def. 1.2.2, Thm. 1.2.7]

$$P(\mathbf{V}) = \prod_{i=1}^{|\mathbf{V}|} P(V_i \mid \text{pa}(V_i)_G). \quad (2)$$

Similarly, we say that an SCM is Markov if it induces a distribution over the observables \mathbf{O} that satisfies (2) [22, Thm. 1.4.1]. If the SCM is not Markov and \mathcal{G} is acyclic, we say that it is *semi-Markov* [22, Ch. 3].

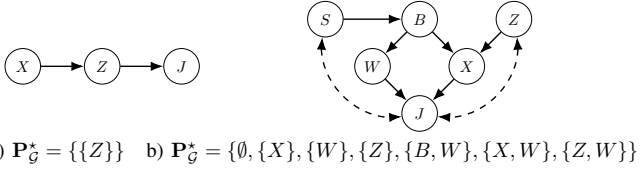
B. Interventions and Causal Effect Identifiability

The operator $\text{do}(\mathbf{X} = \mathbf{x})$ represents an *atomic intervention* that fixes a set of endogenous variable(s) \mathbf{X} to constant value(s) \mathbf{x} irrespective of the functions \mathbf{F} [22, Def. 3.2.1]. Similarly, $\text{do}(\mathbf{X} = \pi(\mathbf{O}))$ represents a *conditional intervention*, whereby the function(s) $\{f_i\}_{i \in \mathbf{X}}$ are replaced with a deterministic function π of the observables. We call such a function an *intervention strategy*.

The standard way to estimate causal effects of interventions [22, Def. 3.2.1] is through controlled experiments [84]. In practice, however, experimentation can be costly and is often not feasible in operational systems. This leads to the fundamental question of whether causal effects can be estimated only from observations. Such estimation can be performed using Pearl’s *do-calculus*, which is an axiomatic system for replacing expressions that contain the do-operator with conditional probabilities [22, Thm. 3.4.1].

In case an SCM includes latent variables [22, Def. 2.3.2], the question of *identifiability* arises:

Definition 1 (Causal effect identifiability [22, Def. 3.2.4]). *The causal effect* [22, Def. 3.2.1] of $\text{do}(\mathbf{X} = \pi(\mathbf{O}))$ on Y is *identifiable* from \mathcal{G} if $P(Y \mid \text{do}(\mathbf{X} = \pi(\mathbf{O})), \mathbf{O})$ is uniquely computable from $P(\mathbf{O}) > 0$ in every SCM conforming to \mathcal{G} .



a) $\mathbf{P}_G^* = \{\{Z\}\}$ b) $\mathbf{P}_G^* = \{\emptyset, \{X\}, \{W\}, \{Z\}, \{B, W\}, \{X, W\}, \{Z, W\}\}$
Fig. 4: Two causal graphs and the corresponding sets of POMISS (Def. 3); J is the target variable, and all other variables are manipulative.

Do-calculus is *complete* in that it allows to derive all identifiable causal effects [22, Cor. 3.4.2][85, Thm. 23]. Consequently, one can prove identifiability by providing a do-calculus derivation that reduces the causal effect to an expression involving only $P(\mathbf{O})$.

C. Automatic Intervention Control

The problem of finding a sequence of conditional interventions $\text{do}(\mathbf{X}_1 = \pi(\mathbf{O})), \dots, \text{do}(\mathbf{X}_{\mathcal{T}} = \pi(\mathbf{O}))$ that maximizes a target variable J can be formulated as a *feedback control problem* [86], also known as a *dynamic treatment regime problem* [87]. We say that such a problem is identifiable if the effect on J caused by every intervention strategy π is identifiable:

Definition 2 (Control problem identifiability [22, Ch. 4.4]). *A control problem with target J and time horizon \mathcal{T} is identifiable from \mathcal{G} if $P(J \mid \text{do}(\mathbf{X}_1 = \pi(\mathbf{O})), \dots, \text{do}(\mathbf{X}_{\mathcal{T}} = \pi(\mathbf{O})))$ is identifiable for each intervention strategy π (Def. 1).*

Given a control problem and a causal graph, we can derive *possibly optimal minimal intervention sets* (POMISS):

Definition 3 (POMIS, adapted from [88, Def. 3]).

Given a control problem with target J and a causal graph \mathcal{G} , $\tilde{\mathbf{X}} \subseteq \mathbf{X}$ is a POMIS if, for each SCM conforming to \mathcal{G} , there is no $\mathbf{X}' \subset \tilde{\mathbf{X}}$ such that $\mathbb{E}_{\pi}[J \mid \text{do}(\tilde{\mathbf{X}} = \tilde{\mathbf{x}})] = \mathbb{E}_{\pi}[J \mid \text{do}(\mathbf{X}' = \mathbf{x}')] \text{ and there exists an SCM such that}$

$$\mathbb{E}_{\pi^*}[J \mid \text{do}(\tilde{\mathbf{X}} = \tilde{\mathbf{x}})] \geq \mathbb{E}_{\pi^*}[J \mid \text{do}(\mathbf{X}' = \mathbf{x}')], \quad (3)$$

for all π , \mathbf{X}' , and \mathbf{x}' , where π^* is an optimal intervention strategy satisfying $\mathbb{E}_{\pi^*}[J] \geq \mathbb{E}_{\pi}[J] \forall \pi$.

Let \mathbf{P}_G^* denote the set of POMISS for a causal graph \mathcal{G} . \mathbf{P}_G^* for two example graphs are shown in Fig. 4. As can be seen in Fig. 4.a, when \mathcal{G} is Markovian, and all variables except the target are manipulative, the only POMIS is the set of parents of the target [88, Prop. 2]. When there are unobserved confounders [22, Def. 6.2.1], however, \mathbf{P}_G^* generally includes many more sets, as shown in Fig. 4.b. An algorithm for computing \mathbf{P}_G^* can be found in [88, Alg. 1].

V. CAUSAL MODEL OF THE CAGE-2 SCENARIO

We model the CAGE-2 scenario by constructing an SCM (1) and formulate the benchmark problem as the problem of finding an optimal intervention strategy for the defender.

A. Target System (Fig. 1)

We represent the physical topology of the target system as a directed graph $\mathcal{G}_S \triangleq (\mathcal{V}, \mathcal{E})$, where nodes represent servers and workstations; edges represent network connectivity. Each node $i \in \mathcal{V}$ is (permanently) located in a zone $z_i \in \mathcal{Z}$ and has three state variables: an intrusion state $I_{i,t}$, a service state $S_{i,t}$, and a decoy state $\mathbf{D}_{i,t}$.

$I_{i,t}$ takes five values: U if the node is unknown to the attacker, K if it is known, S if it has been scanned, C if it is compromised, and R if the attacker has root access (see Fig. 5). Similarly, $S_{i,t}$ takes two values: 1 if the service provided by node i is accessible for clients, 0 otherwise. Lastly, the decoy state $\mathbf{D}_{i,t}$ is a vector $(d_{i,t,1}, \dots, d_{i,t,|\mathcal{D}|})$, where $d_{i,t,j} = 1$ if decoy j is active on node i , 0 otherwise. The set of decoys in CAGE-2 is available in Appendix D and is denoted by \mathcal{D} . The initial state of node i is $(I_{i,1} = \text{U}, S_{i,1} = 1, \mathbf{D}_{i,1} = \mathbf{0})$.

A *workflow graph* \mathcal{G}_W captures service dependencies among nodes (see Appendix D). A directed edge $i \rightarrow j$ in \mathcal{G}_W means that the service provided by node i is used by node j .

B. Attacker

During each time step, the attacker performs an action \mathbf{A}_t , which targets a single node or all nodes in a zone (in case of a scan action). The action is determined by an attacker strategy π_A . It consists of four components $\mathbf{A}_t \triangleq (\alpha_t, V_t, P_t, T_t)$: α_t is the action type, V_t is the vulnerability, $P_t \in \{\text{(U)ser, (R)oof}\}$ is the privileges obtained by exploiting the vulnerability, and T_t is the target, which can be either a single node $i \in \mathcal{V}$ or a zone $z \in \mathcal{Z}$.

There are five attack actions: (S)can, which scans the vulnerabilities of a node; (E)xploit, which attempts to exploit a vulnerability of a node; (P)rivilege escalation, which escalates privileges of a compromised node; (I)mport, which stops the service on a compromised node; and (D)iscover, which discovers the nodes in a zone. These actions have the following causal effects on the intrusion state $I_{i,t}$ and the service state $S_{i,t}$ [22, Def. 3.2.1].

$$\mathbf{A}_{t-1} = f_A(\pi_A, \{I_{i,t-1}\}_{i \in \mathcal{V}}) \quad (4)$$

$$I_{i,t} = f_1(I_{i,t-1}, \mathbf{A}_{t-1}, \mathbf{D}_{i,t}, E_t) \triangleq \quad (5)$$

$$\begin{cases} \text{K if } T_{t-1} = z_i, \alpha_{t-1} = \text{D} \\ \text{K if } T_{t-1} \in \text{pa}(i)_{\mathcal{G}_W}, \alpha_{t-1} = \text{P} \\ \text{S if } T_{t-1} = i, \alpha_{t-1} = \text{S} \\ \text{C if } T_{t-1} = i, \alpha_{t-1} = \text{E}, P_{t-1} = \text{U}, \mathbf{D}_{i,V_t,t} = 0, E_t = 1 \\ \text{R if } T_{t-1} = i, \alpha_{t-1} = \text{E}, P_{t-1} = \text{R}, \mathbf{D}_{i,V_t,t} = 0, E_t = 1 \\ \text{R if } T_{t-1} = i, \alpha_{t-1} = \text{P} \\ I_{i,t-1} \text{ otherwise} \end{cases}$$

$$S_{i,t} = f_S(\mathbf{A}_{t-1}, S_{i,t-1}) \triangleq \begin{cases} 0 & \text{if } T_{t-1} = i, \alpha_{t-1} = \text{I} \\ S_{i,t-1} & \text{otherwise,} \end{cases} \quad (6)$$

where E_t is a binary random variable and $P(E_t = 1)$ is the probability that an exploit at time t is successful (see Fig. 5).

The first two cases in (5) capture the transition $\text{U} \rightarrow \text{K}$, which occurs when the attacker discovers the zone of node i .

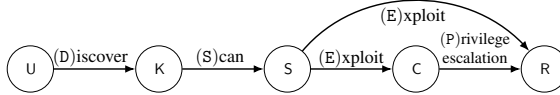


Fig. 5: Transition diagram of the intrusion state $I_{i,t}$ (5); self-transitions are not shown; disks represent states; arrows represent state transitions; labels indicate conditions for state transition; the initial state is $I_{i,1} = U$.

The third case defines the transition $K \rightarrow S$, which happens when the attacker scans the node. The fourth case captures the transition $S \rightarrow C$, which occurs when the attacker compromises the node. The fifth and sixth cases define the transitions $S \rightarrow R$ and $C \rightarrow R$, which occur when the attacker obtains root privileges on the node. The final case captures the recurrent transition $I_{i,t} = I_{i,t-1}$. Lastly, (6) states that the (I)mpact action disrupts the service.

Remark 1. The dependence between (5) and \mathcal{G}_W is unintuitive but is warranted based on the source code of CAGE-2 [4].

C. Observations and Clients

The defender knows the decoy state $\mathbf{D}_{i,t}$ and the service state $S_{i,t}$, but can not observe the intrusion state $I_{i,t}$ nor the attacker action \mathbf{A}_t . Instead of $I_{i,t}$ and \mathbf{A}_t , the defender observes $Z_{i,t}$, which represents network activity at node i .

Like the intrusion state $I_{i,t}$ (5), the activity $Z_{i,t}$ takes five values: (U)nknown, (K)nown, (S)canned, (C)ompromised, and (R)ooot. The value of $Z_{i,t}$ is influenced both by attacker actions and by clients requesting service, which we express as

$$Z_{i,t} = f_{Z,i}(C_t, \mathbf{A}_{t-1}, W_{i,t}), \quad (7)$$

where $W_{i,t} \in \mathbb{N}$ is a noise variable and C_t represents the number of clients requesting service at time t , which is determined as

$$C_t = f_C(C_{t-1}, \mathcal{A}_t, \mathcal{D}_t) \triangleq \max [0, C_{t-1} + \mathcal{A}_t - \mathcal{D}_t], \quad (8)$$

where \mathcal{A}_t and \mathcal{D}_t are the number of clients that arrive and depart in the time interval $[t-1, t]$, respectively.

D. Defender Objective

The defender balances two objectives: maintain services to its clients and minimize the cost of intrusion. In CAGE-2, this bi-objective corresponds to maximizing

$$J = f_J(\{R_t \mid 1 \leq t \leq \mathcal{T}\}) \triangleq \sum_{t=1}^{\mathcal{T}} \gamma^{t-1} R_t \quad (9)$$

$$R_t = f_R(\{I_{i,t}, S_{i,t}\}_{i \in \mathcal{V}}) \triangleq \underbrace{-q_t + \sum_{i \in \mathcal{V}} \psi_{z_i} (S_{i,t} - 1)}_{\text{intervention \& downtime cost}} - \underbrace{\beta_{I_{i,t}, z_i}}_{\text{intrusion cost}},$$

where R_t is the reward at time t ; $q_t \geq 0$ is the intervention cost; $\psi_{z_i} \geq 0$ is the cost of service disruption in zone z_i ; $\beta_{I_{i,t}, z_i} \geq 0$ is the cost of intrusion in zone z_i ; $\gamma \in [0, 1]$ is a discount factor; and \mathcal{T} is the time horizon. The configuration of q_t , ψ_{z_i} , and $\beta_{I_{i,t}, z_i}$ for the target infrastructure in CAGE-2 (Fig. 1) can be found in Appendix C.

Causal model of the CAGE-2 scenario		(M1)
SCM: $\mathcal{M} \triangleq \langle \mathbf{U}, \mathbf{V}, \mathbf{F}, P(\mathbf{U}) \rangle$.		CAUSAL GRAPH: \mathcal{G} (Fig. 6).
TARGET SYSTEM:		
\mathcal{V}, \mathcal{T}	set of nodes and time horizon; see Appendix D	
$\mathcal{G}_S = \langle \mathcal{V}, \mathcal{E} \rangle$	physical topology graph (Fig. 1)	
$\mathcal{G}_W = \langle \mathcal{V}_W \subseteq \mathcal{V}, \mathcal{E}_W \rangle$	workflow graph; see Appendix D.	
RANDOM VARIABLES:		
$\mathbf{U} \triangleq \{E_t, \pi_A, \mathcal{A}_t, \mathcal{D}_t, W_{i,t} \mid i \in \mathcal{V}, 2 \leq t \leq \mathcal{T}\}$		
$\mathbf{V} \triangleq \{I_{i,t}, Z_{i,t}, S_{i,t}, \mathbf{D}_{i,t}, \mathbf{A}_{t>1}, C_t, R_t, J \mid i \in \mathcal{V}, 1 \leq t \leq \mathcal{T}\}$		
$\mathbf{X} \triangleq \{\mathbf{D}_{i,t}, Z_{i,t}, I_{i,t} \mid i \in \mathcal{V}, 1 \leq t \leq \mathcal{T}\}$		
$\mathbf{N} \triangleq (\mathbf{V} \cup \mathbf{U}) \setminus \mathbf{X}$		
$\mathbf{O} \triangleq \{\mathbf{D}_{i,t}, S_{i,t}, Z_{i,t}, C_t \mid i \in \mathcal{V}, 1 \leq t \leq \mathcal{T}\}$		
$\mathbf{L} \triangleq (\mathbf{V} \cup \mathbf{U}) \setminus \mathbf{O}$		
$\mathbf{Y} \triangleq \{R_t, J \mid 1 \leq t \leq \mathcal{T}\}$		
INITIAL CONDITION: $I_{i,1} = Z_{i,1} = U, S_{i,1} = 1, \mathbf{D}_{i,1} = \mathbf{0}, C_1 = R_1 = 0$.		
CAUSAL FUNCTIONS: $\mathbf{F} \triangleq \{f_I, f_S, (f_{Z,i})_{i \in \mathcal{V}}, f_C, f_R, f_J, f_A, f_D\}$.		
OBSERVATIONAL DISTRIBUTIONS:		
$P(\mathbf{U}) = P(\pi_A) \prod_{t=2}^{\mathcal{T}} P(E_t) P(\mathcal{A}_t) P(\mathcal{D}_t) P((W_{i,t})_{i \in \mathcal{V}})$		
$P(\mathbf{V}_t) = \prod_{i=1}^{ \mathcal{V}_t } P(\mathbf{V}_{i,t} \mid \text{pa}(\mathbf{V}_{i,t})_{\mathcal{G}})$.		
INTERVENTIONS: $\text{do}(\widehat{\mathbf{X}}_t = \pi_D(\mathbf{H}_t))$ (10).		

E. Defender Interventions

During each time step, the defender performs an intervention that targets a single node. The defender can make four types of interventions: analyze the node for a possible intrusion, start a decoy service, remove malware, and restore the node to a secure state, which temporarily disrupts its service. We model these interventions as follows.

$$\text{do}(Z_{i,t} = I_{i,t}) \quad \text{analyze}; \quad (10a)$$

$$\text{do}(\mathbf{D}_{i,j,t} = 1) \quad \text{decoy}; \quad (10b)$$

$$\text{do}(I_{i,t} = S) \text{ if } I_{i,t-1} = C \quad \text{remove}; \quad (10c)$$

$$\text{do}(\mathbf{D}_{i,t} = \mathbf{0}, I_{i,t} = S) \text{ if } I_{i,t-1} \in \{C, R\} \quad \text{restore}; \quad (10d)$$

$$\text{do}(\emptyset) \quad \text{none}. \quad (10e)$$

Note that $\mathbf{D}_{i,t}$ remains constant if no interventions occur, i.e., $\mathbf{D}_{i,t} = f_D(\mathbf{D}_{i,t-1}) \triangleq \mathbf{D}_{i,t-1}$.

When selecting interventions, the defender considers the history \mathbf{H}_t , which we define as

$$\mathbf{H}_t \triangleq (\mathbf{V}_1, \text{do}(\widehat{\mathbf{X}}_1), \mathbf{O}_2, \text{do}(\widehat{\mathbf{X}}_2), \dots, \text{do}(\widehat{\mathbf{X}}_{t-1}), \mathbf{O}_t) \quad (11)$$

$$\mathbf{O}_t \triangleq \{\mathbf{D}_{i,t}, S_{i,t}, Z_{i,t}, C_t \mid i \in \mathcal{V}\}, \quad (12)$$

where $\text{do}(\widehat{\mathbf{X}}_t)$ is a shorthand for $\text{do}(\widehat{\mathbf{X}}_t = \widehat{\mathbf{x}}_t)$ and \mathbf{V}_1 is the set of endogenous variables at time t (defined below). The intervention at time t can thus be expressed as $\text{do}(\widehat{\mathbf{X}}_t = \widehat{\mathbf{x}}_t)$, where π_D is a *defender strategy*.

Remark 2. The fact that the defender remembers the history \mathbf{H}_t (11) means that it has *perfect recall* [89, Def. 7].

F. A Structural Causal Model of CAGE-2

The variables and the causal functions (4)–(9) described above determine the SCM (1) defined in (M1). Notable properties of (M1) are a) the causal graph is acyclic (see Fig. 6); b)

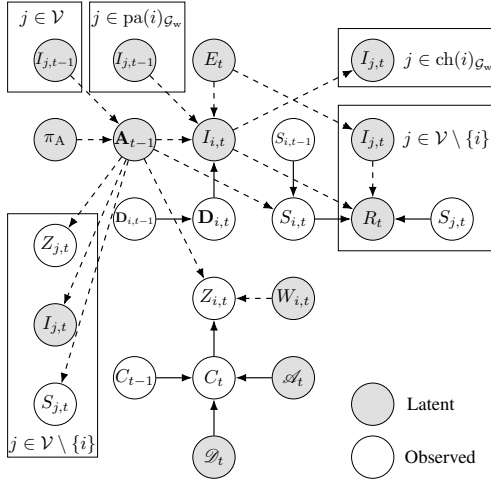


Fig. 6: Causal (summary) graph of (M1) for node i [90, Ch. 10]; plate notation is used to represent sets of variables [91].

the model is *stationary*; c) the model is *semi-Markov* [22, Thm. 1.4.1]; d) the exogeneous variables are jointly independent; and e) $P(\mathbf{V}_t)$ is Markov relative to \mathcal{G} (2) [22, Thm. 1.2.7].

The size of the causal graph \mathcal{G} associated with (M1) grows linearly with the time horizon \mathcal{T} and with the number of nodes in the target system $|\mathcal{V}|$. A summary of \mathcal{G} is shown in Fig. 6.

G. The Defender Problem in CAGE-2

Given (M1) and the defender objective (9), the problem for the defender can be stated as follows.

Problem 1 (Optimal defender strategy in CAGE-2 (M1)).

$$\underset{\pi_D}{\text{maximize}} \quad \mathbb{E}_{\pi_D} [J \mid \mathbf{V}_1] \quad (13a)$$

$$\text{subject to} \quad \text{do}(\widehat{\mathbf{X}}_t = \pi_D(\mathbf{h}_t)) \quad \forall t \quad (13b)$$

$$\pi_A \sim P(\pi_A) \quad \forall t \quad (13c)$$

$$\mathcal{A}_t \sim P(\mathcal{A}_t), \mathcal{D}_t \sim P(\mathcal{D}_t) \quad \forall t \quad (13d)$$

$$E_t \sim P(E_t), W_{i,t} \sim P(W_{i,t}) \quad \forall t, i \quad (13e)$$

$$\mathbf{A}_t = f_A(\pi_A, \{I_{i,t}\}_{i \in \mathcal{V}}) \quad \forall t, i \quad (13f)$$

$$\mathbf{D}_{i,t} = f_D(\mathbf{D}_{i,t-1}) \quad \forall t, i \quad (13g)$$

$$I_{i,t} = f_I(I_{i,t-1}, \mathbf{A}_{t-1}, \mathbf{D}_{i,t}, E_t) \quad \forall t, i \quad (13h)$$

$$Z_{i,t} = f_Z(C_t, \mathbf{A}_{t-1}, W_{i,t}) \quad \forall t, i \quad (13i)$$

$$C_t = f_C(C_{t-1}, \mathcal{A}_t, \mathcal{D}_t) \quad \forall t \quad (13j)$$

$$S_{i,t} = f_S(\mathbf{A}_{t-1}, S_{i,t-1}) \quad \forall t, i \quad (13k)$$

$$R_t = f_R(\{I_{i,t}, S_{i,t}\}_{i \in \mathcal{V}}) \quad \forall t \quad (13l)$$

$$J = f_J(\{R_t\}_{t=1, \dots, \mathcal{T}}) \quad (13m)$$

where (13b) defines the interventions; (13d)–(13e) capture the distribution of \mathbf{U} ; and (13f)–(13m) define \mathbf{F} .

We say that a *defender strategy* π_D^* is *optimal* if it solves Prob. 1. This problem is well-defined in the following sense.

Theorem 1. *Assuming $C_t, \mathcal{A}, \mathcal{V}, q_t, \beta_{I_{i,t}, z}, \psi_z$, are finite, and \mathcal{T} is finite or $\gamma < 1$, then there exists an optimal deterministic defender strategy π_D^* . If $\mathcal{T} = \infty$, then there exists a π_D^* that is stationary.*

Proof. For notational convenience, let $\mathbf{S}_t \triangleq \{S_{i,t}\}_{i \in \mathcal{V}}$, $\mathbf{I}_t \triangleq \{I_{i,t}\}_{i \in \mathcal{V}}$, $\mathbf{D}_t \triangleq \{\mathbf{D}_{i,t}\}_{i \in \mathcal{V}}$, $\mathbf{W}_t \triangleq \{W_{i,t}\}_{i \in \mathcal{V}}$, and $\mathbf{Z}_t \triangleq \{Z_{i,t}\}_{i \in \mathcal{V}}$. We break down the proof into the following steps.

1) $\Sigma_t \triangleq (\mathbf{I}_t, \mathbf{D}_t, C_t, \mathbf{A}_{t-1}, \pi_A, \mathbf{S}_{t-1})$ is Markovian.

PROOF:

$$\begin{aligned} P(\Sigma_{t+1} \mid \Sigma_1, \dots, \Sigma_t) &= P(\mathbf{A}_t \mid \pi_A, \mathbf{I}_t) P(\mathcal{A}_{t+1}) P(\mathcal{D}_{t+1}) \times \\ P(C_{t+1} \mid \mathcal{A}_{t+1}, \mathcal{D}_{t+1}, C_t) P(E_{t+1}) P(\mathbf{S}_{t+1} \mid \mathbf{S}_t, \mathbf{A}_t) \times \\ P(\mathbf{I}_{t+1} \mid \mathbf{I}_t, \mathbf{A}_t, \mathbf{D}_{t+1}, E_{t+1}) = P(\Sigma_{t+1} \mid \Sigma_t). \end{aligned}$$

2) $(\mathbf{O}_t, R_t \perp\!\!\!\perp \{\mathbf{V}_t\}_{t=1, \dots, t} \mid \Sigma_t)$.

PROOF:

$$\begin{aligned} P(\mathbf{O}_t, R_t \mid \{\mathbf{V}_t\}_{t=1, \dots, t}) &= P(\mathbf{Z}_t \mid C_t, \mathbf{A}_{t-1}, \mathbf{W}_t) \times \\ P(\mathbf{W}_t) P(\mathbf{S}_t \mid \mathbf{S}_{t-1}, \mathbf{A}_{t-1}) P(R_t \mid \mathbf{I}_t, \mathbf{S}_t) = P(\mathbf{O}_t, R_t \mid \Sigma_t). \end{aligned}$$

3) $\text{dom}(\mathbf{O}_t)$, $\text{dom}(\Sigma_t)$, and R_t are finite.

PROOF: Follows from the theorem assumptions.

4) Each defender strategy π_D induces a well-defined probability measure over the random sequence $(\Sigma_t, \mathbf{O}_t)_{t \geq 1}$.

PROOF: 3) implies that the sample spaces of (Σ_t, \mathbf{O}_t) and $(\Sigma_t, \mathbf{O}_t)_{t \geq 1}$ are measurable and countable, respectively. Further, the fact that \mathcal{G} is acyclic implies that the interventional distributions induced by $(\text{do}(\widehat{\mathbf{X}}_t = \widehat{\mathbf{x}}_t))_{t \geq 1}$ are well-defined [22, Ch. 3]. Consequently, the statement follows from the Ionescu-Tulcea extension theorem [92].

5) $P(\Sigma_{t+1} \mid \Sigma_t)$, $P(\mathbf{O}_t \mid \Sigma_t)$, and $P(R_t \mid \Sigma_t)$ are stationary.

PROOF: Follows by stationarity of (M1).

Statements 1–5 imply that Prob. 1 defines a finite, stationary, and partially observed Markov decision process (POMDP) with bounded rewards. The theorem thus follows from standard results in Markov decision theory, see [93, Thm. 7.6.1]. \square

Theorem 1 states that an optimal defender strategy π_D^* exists. Finding such a strategy requires estimating the causal effect $P(J \mid \text{do}(\widehat{\mathbf{X}}_1 = \pi_D(\mathbf{H}_1)), \dots, \text{do}(\widehat{\mathbf{X}}_{\mathcal{T}} = \pi_D(\mathbf{H}_{\mathcal{T}})))$ for different strategies π_D [22, Def. 3.2.1]. A key question is thus whether the effect is identifiable, i.e., whether it can be estimated from the observables. The following theorem states that the answer is negative.

Theorem 2. *Problem 1 is not identifiable (Def. 2).*

Proof. To prove non-identifiability, it is sufficient to present two sets of causal functions $\mathbf{F}', \mathbf{F}''$ that induce identical distributions over the observables but have different causal effects (Def. 2) [22] [94, Lem. 1]. For simplicity, consider $\mathcal{T} = 2$ and $|\mathcal{V}| = 1$. In this case $J = R$ (9). Let

$$\begin{aligned} \mathbf{F}' &\triangleq \{f_R(S, I) \triangleq \mathbb{1}_{I=R}, f_I(\mathbf{A}, E, \mathbf{D}) = R, \\ &f_S(S, \mathbf{A}) = 1, f_Z, f_C, f_J, f_A, f_D\}, \end{aligned}$$

where $\{f_Z, f_C, f_J, f_A, f_D\}$ are defined arbitrarily. Now let \mathbf{F}'' be equivalent to \mathbf{F}' except for $f_R(S, I) \triangleq S$. Clearly $P(\mathbf{O})$ is the same with both \mathbf{F}' and \mathbf{F}'' . However, $P(J = 0 \mid \text{do}(I = S)) = 1$ with \mathbf{F}' but $P(J = S \mid \text{do}(I = S)) = 1$ with \mathbf{F}'' . \square

Theorem 2 states that causal effects of defender interventions (10) can *not* be identified from observations. This statement is obvious in hindsight but has important ramifications. It implies that to evaluate a defender strategy π_D , the defender

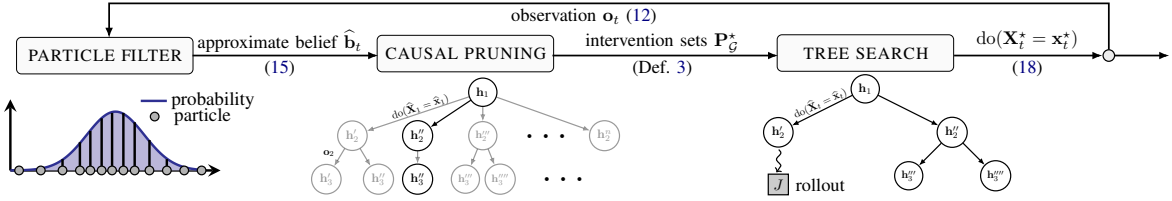


Fig. 7: Causal Partially Observed Monte-Carlo Planning (C-POMCP, Alg. 1); the figure illustrates one time step during which (i) a particle filter is used to compute an approximate belief state \hat{b}_t (14); (ii) a causal graph [22, Def. 2.2.1] (see Fig. 6) is used to prune the search tree of possible histories h_k (11) by only considering histories with interventions in POMISS (see Def. 3); and (iii) tree search is used to find an optimal intervention $\text{do}(\mathbf{X}_t^* = \mathbf{x}_t^*)$ (18).

must either know (M1) or perform controlled experiments to measure the effects of the interventions prescribed by π_D .

While it is likely that the defender is aware of certain components of (M1), it is unrealistic that it knows the entire model. A more reasonable assumption is that the defender knows the causal graph \mathcal{G} (Fig. 6), which does not capture all nuances of the causal mechanisms but provides structural information. Leveraging this structure, we next present a method for finding an optimal strategy π_D^* which only requires access to the causal graph and a simulator of (M1).

Remark 3. Access to a simulator is assumed by virtually all existing methods for autonomous cyber defense [5]–[20].

VI. CAUSAL PARTIALLY OBSERVABLE MONTE-CARLO PLANNING (C-POMCP)

In this section, we present C-POMCP, an online method for obtaining an optimal defender strategy π_D^* for Prob. 1. The method involves three consecutive actions that are performed at each time step t (see Fig. 7).

The first action uses the observation \mathbf{o}_t and a *particle filter* to compute the defender's *belief* \hat{b}_t in the form of a probability distribution over the latent variables \mathbf{L} in (M1). The second action constructs a *search tree* of possible future histories h_k (11), which is initialized with a root node that represents the current history h_t . Each edge extends this history by either an observation or an intervention: if h_{k+1} is a child node of h_k , then either $h_{k+1} = (h_k, \mathbf{o}_{k+1})$ or $h_{k+1} = (h_k, \text{do}(\tilde{\mathbf{X}}_k = \hat{\mathbf{x}}_k))$. C-POMCP then *prunes* the tree by *excluding* histories that contain interventions that do not belong to a POMIS (Def. 3). The third action uses the belief \hat{b}_t and the pruned tree to perform *Monte-Carlo tree search*, which involves estimating the reward J (9) through simulations. Once the search has been completed, the intervention from the root node that leads to the highest value of J (9) is returned. The pseudocode of C-POMCP is listed in Alg. 1, and the main components of the method are described below.

A. Particle Filtering to Estimate Latent Variables

The particle filter is a method for state estimation in partially observed dynamical systems [95]. Since (M1) can be formulated as such a system (Thm. 1), we use the particle filter to estimate the values of the latent variables \mathbf{L} in (M1), e.g., the intrusion state $I_{i,t}$ (5).

We define the defender's *belief state* as

$$\mathbf{b}_t(\sigma_t) \triangleq P(\Sigma_t = \sigma_t \mid \mathbf{h}_t) \quad (14)$$

$$\begin{aligned} &\stackrel{\text{(Bayes)}}{=} \eta P(\mathbf{o}_t \mid \sigma_t, \mathbf{h}_{t-1}) P(\sigma_t \mid \text{do}(\tilde{\mathbf{X}}_t = \hat{\mathbf{x}}_t), \mathbf{h}_{t-1}) \\ &\stackrel{\text{(Markov)}}{=} \eta P(\mathbf{o}_t \mid \sigma_t) P(\sigma_t \mid \text{do}(\tilde{\mathbf{X}}_t = \hat{\mathbf{x}}_t), \mathbf{h}_{t-1}) \\ &\stackrel{\text{(Markov)}}{=} \eta P(\mathbf{o}_t \mid \sigma_t) \sum_{\sigma_{t-1}} P(\sigma_t \mid \sigma_{t-1}, \text{do}(\tilde{\mathbf{X}}_t = \hat{\mathbf{x}}_t)) \mathbf{b}_{t-1}(\sigma_{t-1}), \end{aligned}$$

where \mathbf{h}_t is the history (11), σ_t is a realization of Σ_t (see Thm. 1), and η is a normalizing constant. The sum in (14) is over all possible realizations of Σ_{t-1} .

The computational complexity of (14) is $\mathcal{O}(|\text{dom}(\Sigma)|^2)$, which grows quadratically with the size of the state space and exponentially with the number of state variables. For this reason, the particle filter approximates (14) by representing \mathbf{b}_t by a set of M sample states (particles) $\mathcal{P}_t = \{\hat{\sigma}_t^{(1)}, \dots, \hat{\sigma}_t^{(M)}\}$ [96]. These particles are sampled recursively as

$$\bar{\mathcal{P}}_t \triangleq \bigcup_{i=1}^M \left\{ \hat{\sigma}_t^{(i)} \sim P \left(\cdot \mid \hat{\sigma}_{t-1}^{(i)}, \text{do}(\tilde{\mathbf{X}}_{t-1} = \hat{\mathbf{x}}_{t-1}) \right) \right\} \quad (15a)$$

$$\mathcal{P}_t \triangleq \bigcup_{i=1}^M \left\{ \hat{\sigma}_t^{(i)} \stackrel{\propto P(\mathbf{o}_t \mid \hat{\sigma}_t^{(i)})}{\sim} \bar{\mathcal{P}}_t \right\}, \quad (15b)$$

where $\hat{\sigma}_{t-1}^{(i)} \in \mathcal{P}_{t-1}$ and $x \stackrel{\propto}{\sim}$ means that x is sampled with probability proportional to φ .

(15a)–(15b) focus the particle set to regions of the state space with a high probability of generating the latest observation \mathbf{o}_t [95]. This ensures that the belief state induced by the particles converges to (14) when $M \rightarrow \infty$, as stated below.

Theorem 3. Let $\hat{\mathbf{b}}(\sigma_t) = \frac{1}{M} \sum_{i=1}^M \mathbb{1}_{\sigma_t = \hat{\sigma}_t^{(i)}}$, then

$$\lim_{M \rightarrow \infty} \hat{\mathbf{b}}_t \rightarrow \mathbf{b}_t \text{ almost surely} \quad \forall t.$$

This is a standard result in particle filtering. The proof is given in Appendix A.

B. Causal Pruning of the Search Tree

We use the causal graph \mathcal{G} (Fig. 6) to prune the search tree by excluding histories h_k (11) that contain interventions that do not belong to a POMIS \mathbf{P}_G^* (Def. 3). For example, when $t = \mathcal{T} - 1$, then $Z_{i,t}$ (7) and J (9) are *d-separated* in \mathcal{G} [22, Def. 1.2.3]. This means that the intervention $\text{do}(Z_{i,t} = I_{i,t})$ (10a) has no causal effect on J and thus $Z_{i,t} \notin \mathbf{P}_G^*$.

By restricting the possible interventions at time t to the set of POMISS \mathbf{P}_G^* , the number of interventions in the search tree is reduced by a factor of

$$\prod_{t=1}^{\mathcal{T}} \frac{\sum_{\tilde{\mathbf{X}} \in \mathbf{P}_G^*} |\text{dom}(\tilde{\mathbf{X}})|}{\sum_{\hat{\mathbf{X}} \in \mathbf{2}^{\mathbf{X}_t}} |\text{dom}(\hat{\mathbf{X}})|}, \quad (16)$$

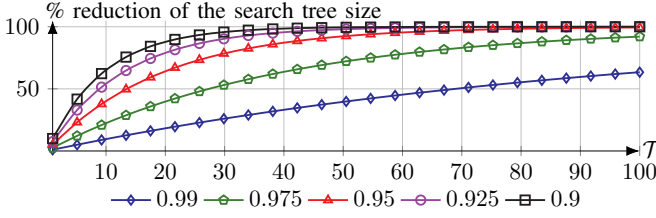


Fig. 8: Reduction of the size of the search tree by pruning the intervention space $|2^{\mathbf{X}_t}|$ to the set of POMISS \mathbf{P}_G^* (Def. 3); the x-axis indicates the tree depth T ; curves relate to the factor in (16).

where \mathbf{X}_t is the set of manipulative variables at time t (M1).

Hence, even if only a small subset of interventions does not belong to an POMIS, a significant reduction in the search tree size can be expected (see Fig. 8). Unfortunately, computing \mathbf{P}_G^* is generally intractable, as stated below.

Proposition 1. *Computing \mathbf{P}_G^* (Def. 3) is PSPACE-hard.*

Proof. We prove the PSPACE-hardness by reduction to the problem of solving a POMDP, which is PSPACE-hard [97, Thm. 6]. Let x be an instance of the problem of computing \mathbf{P}_G^* (Def. 3). Finding a solution to x involves checking (3) for each $\tilde{\mathbf{X}}_t \in \mathbf{P}_G^*$. This means that a solution to x allows constructing an optimal solution to Prob. 1. By Thm 1, such a solution also provides a solution to a POMDP. \square

Given the impracticality of computing \mathbf{P}_G^* (Prop. 1), we approximate \mathbf{P}_G^* as follows. First, we reduce the causal graph to a subgraph $\mathcal{G}[\mathbf{U}_{t-1} \cup \mathbf{U}_t \cup \mathbf{V}_{t-1} \cup \mathbf{V}_t]$ [22, Def. 7.1.2]. We then remove all variables in the subgraph whose values are uniquely determined by $\hat{\mathbf{b}}$ (15). Subsequently, we add a node to the subgraph that represents the target J (9), whose causal parents [22, Def. 1.2.1] are determined using a *base strategy* $\hat{\pi}$, which can be chosen freely. It can, for example, be based on heuristics or be designed by a domain expert. Finally, we compute a POMIS for the reduced graph using [88, Alg. 1].

Remark 4. Since [88, Alg. 1] is sound and complete [88, Thm. 9], the approximation described above is exact when the base strategy $\hat{\pi}$ is optimal.

When applying the above procedure to the CAGE-2 scenario, we identify the following types of defender interventions that are never included in a POMIS: (i) interventions that start decoys that are already running; (ii) defensive interventions on nodes that are not compromised according to $\hat{\mathbf{b}}$ (15); and (iii) forensic and deceptive interventions on nodes that are compromised according to $\hat{\mathbf{b}}$ (15).

Remark 5. The pruning of the search tree based on the POMISS (Def. 3) occurs *during* the construction of the tree. The complete search tree is generally too large to construct.

C. Monte-Carlo Tree Search

Given the particle filter (14) and the POMIS (Def. 3), C-POMCP searches for optimal interventions using the tree search algorithm described in [24, Alg. 1]. This algorithm constructs a search tree iteratively by repeating five steps (see Fig. 9): (i) it

selects a path from the root to a leaf node using the *tree policy* described below; (ii) it expands the tree by adding children to the leaf, each of which corresponds to an intervention (10) on a POMIS (Def. 3); (iii) it executes a rollout simulation from the leaf; (iv) it adds a child to the leaf that corresponds to the first observation (12) in the simulation; and (v) it records the value of J (9) and backpropagates the value up the tree.

Tree policy. A node at depth k of the tree is associated with a history \mathbf{h}_k (11) and stores two variables: the average cumulative reward $\hat{J}(\mathbf{h}_k)$ (9) of simulations on the subtree emanating from the node, and the visit count $N(\mathbf{h}_k) \geq 1$, which is incremented whenever the node is visited during the search. Using these variables, we implement the tree policy by selecting nodes that maximize the upper confidence bound

$$\hat{J}(\mathbf{h}_k) + c \sqrt{\frac{\ln N(\mathbf{h}_{k-1})}{N(\mathbf{h}_k)}}, \quad (17)$$

where $c > 0$ controls the exploration-exploitation trade-off.

Rollout. The initial state of a rollout simulation is sampled from the belief state $\hat{\mathbf{b}}_k$ (15), and the intervention at each time step is selected using the *base strategy* $\hat{\pi}$ (§VI-B). The simulation executes for a depth of δ_R , after which the reward for the remainder of the simulation is estimated using a *base value function* $J_{\hat{\pi}}$. Like the base strategy, this function can be chosen freely. It can, for example, be obtained through offline reinforcement learning. After the simulation has completed, the discounted sum of the rewards $R_1, R_t, \dots, R_{\delta_R}$ (9) and $J_{\hat{\pi}}$ is used to update $\hat{J}(\mathbf{h}_k)$.

Convergence. The process of running simulations and extending the search tree continues for a *search time* s_T , after which the intervention that leads to the maximal value of J (9) is returned, i.e.,

$$\text{do}(\tilde{\mathbf{X}}_t = \tilde{\mathbf{x}}_t) \in \arg \max_{\text{do}(\tilde{\mathbf{X}}_t = \hat{\mathbf{x}}_t)} \hat{J}((\mathbf{h}_t, \text{do}(\tilde{\mathbf{X}}_t = \hat{\mathbf{x}}_t))).$$

We can express this search procedure as

$$\text{do}(\tilde{\mathbf{X}}_t = \tilde{\mathbf{x}}_t) \leftarrow \mathcal{T}(\mathbf{h}_t, \hat{\mathbf{b}}_t, \hat{\pi}, s_T, \mathcal{S}, \mathcal{G}, \mathbf{P}_G^*), \quad (18)$$

where \mathcal{T} is a tree search operator.

Theorem 4. *Under the assumptions made in Thm. 1 and further assuming that the POMIS computation is exact (§VI-B), $M \rightarrow \infty$, $s_T \rightarrow \infty$, $T < \infty$, and c is chosen such that*

$$P \left(\hat{J}(\mathbf{h}_k) \leq \mathbb{E}[\hat{J}(\mathbf{h}_k)] \pm c \sqrt{\frac{\ln N(\mathbf{h}_{k-1})}{N(\mathbf{h}_k)}} \right) \leq k^{-4} \quad (19)$$

for all $k \geq 1$. Then the intervention prescribed by C-POMCP (18) for any \mathbf{h}_t converges in probability to an optimal intervention $\text{do}(\mathbf{X}_t^* = \mathbf{x}_t^*)$.

The proof of Thm. 4 relies on mapping an execution of C-POMCP to an execution of the UCT algorithm [98, Fig. 1], which is known to converge as $s_T \rightarrow \infty$ [98, Thm. 7]. We provide the proof in Appendix B. Note that (19) can always be satisfied by choosing a large c .

Remark 6. Theorem 4 is not confined to CAGE-2 (M1). Rather, the theorem is general and applies to any control

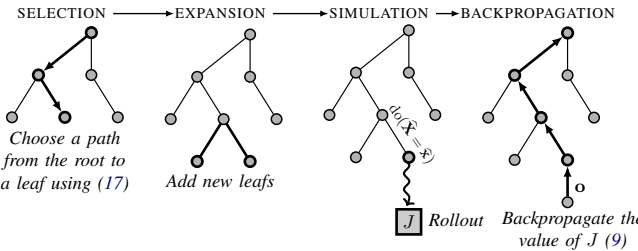


Fig. 9: Tree search in C-POMCP; a search tree is constructed iteratively where each iteration consists of the four phases above.

problem based on an SCM with interventions that can be formulated as a finite and stationary POMDP (Thm. 1).

Algorithm 1: C-POMCP.

```

1 Input: Simulator  $\mathcal{S}$  of (M1), causal graph  $\mathcal{G}$  (Fig. 6),
2   search time  $s_T$ , horizon  $\mathcal{T}$ , number of particles  $M$ .
3 Output: Interventions  $\text{do}(\tilde{\mathbf{X}}_1 = \tilde{\mathbf{x}}_1), \dots, \text{do}(\tilde{\mathbf{X}}_{\mathcal{T}} = \tilde{\mathbf{x}}_{\mathcal{T}})$ .
4 Algorithm
5    $\mathbf{h}_1 = (\mathbf{V}_1,)$ .
6   for  $t = 1, 2, \dots, \mathcal{T}$  do
7     Compute  $\hat{\mathbf{b}}_t$  using (15) with  $M$  particles.
8     Compute  $\mathbf{P}_G^*$  (Def. 3).
9      $\text{do}(\tilde{\mathbf{X}}_t = \tilde{\mathbf{x}}_t) \leftarrow \mathcal{I}(\mathbf{h}_t, \hat{\mathbf{b}}_t, \hat{\pi}, s_T, \mathcal{S}, \mathcal{G}, \mathbf{P}_G^*)$  (18).
10    Perform intervention  $\text{do}(\tilde{\mathbf{X}}_t = \tilde{\mathbf{x}}_t)$  (10).
11    Observe  $\mathbf{o}_{t+1}$ .
12    Update history  $\mathbf{h}_{t+1} = (\mathbf{h}_t, \text{do}(\tilde{\mathbf{X}}_t = \tilde{\mathbf{x}}_t), \mathbf{o}_{t+1})$  (11).
13 end

```

D. Comparison with Other Methods

C-POMCP (Alg. 1) distinguishes itself from existing methods evaluated against the CAGE-2 benchmark ([5]–[13], [16]–[20]) in four key aspects. First, it incorporates the causal structure of the target system. Second, it guarantees an optimal solution (Thm. 4). No such guarantees are available for the existing methods. Third, while the above-referenced methods ignore the latent variables, C-POMCP explicitly models the uncertainty of the latent variables and how this uncertainty changes in light of new observations (14). Fourth, in contrast to the existing *offline* methods, C-POMCP is an *online* method that updates the defender strategy at each time step.

VII. EVALUATING C-POMCP AGAINST CAGE-2

We implement C-POMCP (Alg. 1) in Python and run it to learn defender strategies for the CAGE-2 scenario [4]. The source code is available at [25]; the system configuration is listed in Appendix D; the hyperparameters are listed in Appendix C; and the computing environment is an M2-ultra processor.

Baselines. We compare the performance of C-POMCP (Alg. 1) with that of two baselines: CARDIFF-PPO, a current state-of-the-art method for CAGE-2 [5], and POMCP [24, Alg. 1], a non-causal version C-POMCP. Note that, while we only compare against CARDIFF-PPO from the CAGE-2 leaderboard, it represents all methods on the leaderboard since it achieves better performance than the other methods [4].

Evaluation metrics. We use two evaluation metrics: the cumulative reward $\mathbb{E}[J]$ (9) and the cumulative regret [99]

$$\mathfrak{R}_n \triangleq n\mathbb{E}_{\pi_D^*}[J] - \mathbb{E}_{\pi_{n,D}} \left[\sum_{l=1}^n J_l \right], \quad (20)$$

where n is the total computational time in minutes, J_l is the value of (9) achieved after l minutes, and $\pi_{n,D} = (\pi_{1,D}, \pi_{2,D}, \dots, \pi_{n,D})$ represents the sequence of defender strategies after n minutes of computations (e.g., n minutes of tree search) [99]. Since computing $\mathbb{E}_{\pi_D^*}[J]$ is PSPACE-hard [97, Thm. 6], we estimate $\mathbb{E}_{\pi_D^*}[J]$ using the current state-of-the-art value when computing (20).

A. CAGE-2 Scenarios

The CAGE-2 scenario can be instantiated with different attacker strategies π_A (4) as well as different topologies within each zone (see Fig. 1) [4]. Based on these parameters, we define the following evaluation scenarios.

Scenario 1 (B-LINE attacker). In this scenario, the attacker strategy π_A represents the B-LINE attacker from CAGE-2 [4], which attempts to move directly to the operational zone. The topology is shown in Fig. 1.

Scenario 2 (MEANDER attacker). In this scenario, π_A represents the MEANDER attacker from CAGE-2 [4]. MEANDER explores the network one zone at a time, seeking to gain privileged access to all hosts in a zone before moving on to the next one, eventually arriving at the operational zone. The topology is shown in Fig. 1.

Scenario 3 (RANDOM attacker). In this scenario, π_A is B-LINE with probability 0.5 and MEANDER with probability 0.5. The topology is shown in Fig. 1.

Scenario 4 (RANDOM topology). This scenario is the same as Scenario 1 except that the topologies of the enterprise and user zones are randomized at the start of each evaluation episode.

B. CAGE-2 Benchmark Results

The evaluation results are summarized in Figs. 10–11 and Tables 2–3. The results show that C-POMCP (Alg. 1) achieves the highest reward (9) and the lowest regret (20) across all evaluation scenarios and time horizons \mathcal{T} . (The results are not statistically significant in all cases, though.)

The green curves in Fig. 10 relate to C-POMCP. The blue and red curves relate to the baselines. The leftmost column in Fig. 10 shows the regret (20). Notably, the regret of C-POMCP is two orders of magnitude lower than the regret of CARDIFF-PPO and one order of magnitude lower than the regret of POMCP.

The three rightmost columns in Fig. 10 show the cumulative reward (9) obtained by C-POMCP and POMCP in function of the search time s_T . We observe that C-POMCP achieves a significantly higher reward than POMCP, although the difference diminishes with increasing s_T , which is expected (Thm. 4). We explain the improvement of C-POMCP compared to POMCP by the pruned search tree, which is obtained by leveraging the causal structure (Def. 3). The reduction in search tree size

Method	Training / search (minutes) (seconds)	$\mathcal{T} = 30$			$\mathcal{T} = 50$			$\mathcal{T} = 100$		
		SCENARIO 1	SCENARIO 2	SCENARIO 3	SCENARIO 1	SCENARIO 2	SCENARIO 3	SCENARIO 1	SCENARIO 2	SCENARIO 3
CARDIFF	2000 / 10 ⁻⁴	-3.57 ± 0.06	-5.69 ± 1.68	-4.76 ± 1.90	-6.44 ± 0.16	-9.23 ± 2.87	-7.64 ± 2.78	-13.69 ± 0.533	-17.16 ± 4.41	-15.28 ± 4.18
C-POMCP	0 / 0.05	-4.64 ± 0.5	-5.73 ± 0.08	-5.18 ± 0.13	-9.20 ± 0.38	-9.35 ± 0.16	-9.27 ± 0.67	-25.05 ± 3.02	-18.29 ± 0.13	-21.67 ± 3.19
C-POMCP	0 / 0.1	-3.89 ± 0.25	-5.62 ± 0.14	-4.75 ± 0.34	-8.46 ± 0.27	-8.92 ± 0.23	-8.69 ± 0.47	-21.28 ± 0.72	-17.38 ± 0.20	-19.33 ± 1.03
C-POMCP	0 / 0.5	-4.00 ± 0.14	-5.61 ± 0.02	-4.81 ± 0.24	-7.38 ± 0.19	-8.62 ± 0.18	-8.00 ± 0.44	-18.08 ± 1.32	-16.81 ± 0.14	-17.45 ± 1.14
C-POMCP	0 / 1	-3.64 ± 0.13	-5.52 ± 0.16	-4.58 ± 0.27	-6.60 ± 0.32	-8.55 ± 0.08	-7.58 ± 0.29	-17.42 ± 1.08	-16.34 ± 0.44	-16.88 ± 1.29
C-POMCP	0 / 5	-3.50 ± 0.11	-5.65 ± 0.11	-4.57 ± 0.23	-6.52 ± 0.34	-8.46 ± 0.11	-7.49 ± 0.46	-13.23 ± 0.43	-16.46 ± 0.30	-14.85 ± 0.79
C-POMCP	0 / 15	-3.37 ± 0.08	-5.66 ± 0.11	-4.52 ± 0.19	-6.57 ± 0.38	-8.57 ± 0.13	-7.57 ± 0.52	-12.98 ± 1.55	-15.87 ± 0.67	-14.43 ± 1.99
C-POMCP	0 / 30	-3.42 ± 0.09	-5.70 ± 0.09	-4.56 ± 0.14	-6.34 ± 0.28	-8.52 ± 0.18	-7.43 ± 0.52	-13.32 ± 0.18	-16.05 ± 0.96	-14.68 ± 1.02
POMCP	0 / 0.05	-6.87 ± 0.21	-9.50 ± 0.19	-8.19 ± 0.37	-13.90 ± 0.24	-22.26 ± 0.44	-18.08 ± 0.72	-38.71 ± 1.99	-50.24 ± 2.67	-44.48 ± 3.11
POMCP	0 / 0.1	-6.31 ± 0.12	-8.70 ± 0.07	-7.51 ± 0.19	-13.71 ± 0.22	-20.20 ± 0.47	-16.96 ± 0.76	-38.02 ± 0.53	-46.40 ± 0.64	-42.21 ± 0.79
POMCP	0 / 0.5	-5.32 ± 0.24	-8.28 ± 0.13	-6.80 ± 0.33	-12.89 ± 0.20	-19.16 ± 0.09	-16.03 ± 0.33	-34.92 ± 0.96	-47.29 ± 0.39	-41.11 ± 1.23
POMCP	0 / 1	-5.27 ± 0.65	-7.68 ± 0.10	-6.48 ± 0.75	-12.57 ± 0.41	-18.38 ± 0.50	-15.48 ± 0.94	-34.50 ± 0.65	-47.02 ± 1.75	-40.76 ± 2.34
POMCP	0 / 5	-5.11 ± 0.32	-7.58 ± 0.05	-6.35 ± 0.36	-12.03 ± 0.93	-18.22 ± 0.19	-15.13 ± 1.18	-33.06 ± 0.21	-45.15 ± 0.54	-39.13 ± 0.66
POMCP	0 / 15	-5.18 ± 0.66	-7.30 ± 0.38	-6.24 ± 1.22	-11.32 ± 0.84	-17.68 ± 0.58	-14.50 ± 1.37	-30.88 ± 1.41	-45.19 ± 0.35	-38.04 ± 1.57
POMCP	0 / 30	-4.50 ± 0.17	-6.92 ± 0.59	-5.71 ± 0.77	-9.88 ± 1.63	-17.55 ± 0.44	-13.72 ± 2.09	-29.51 ± 2.00	-44.27 ± 1.13	-36.89 ± 2.49

TABLE 2: Comparing C-POMCP with baselines: CARDIFF-PPO [5] and POMCP [24]; columns indicate the time horizon \mathcal{T} (9); subcolumns indicate the evaluation scenario (§VII-A); numbers indicate the mean and the standard deviation of the reward J (9) from evaluations with 3 random seeds.

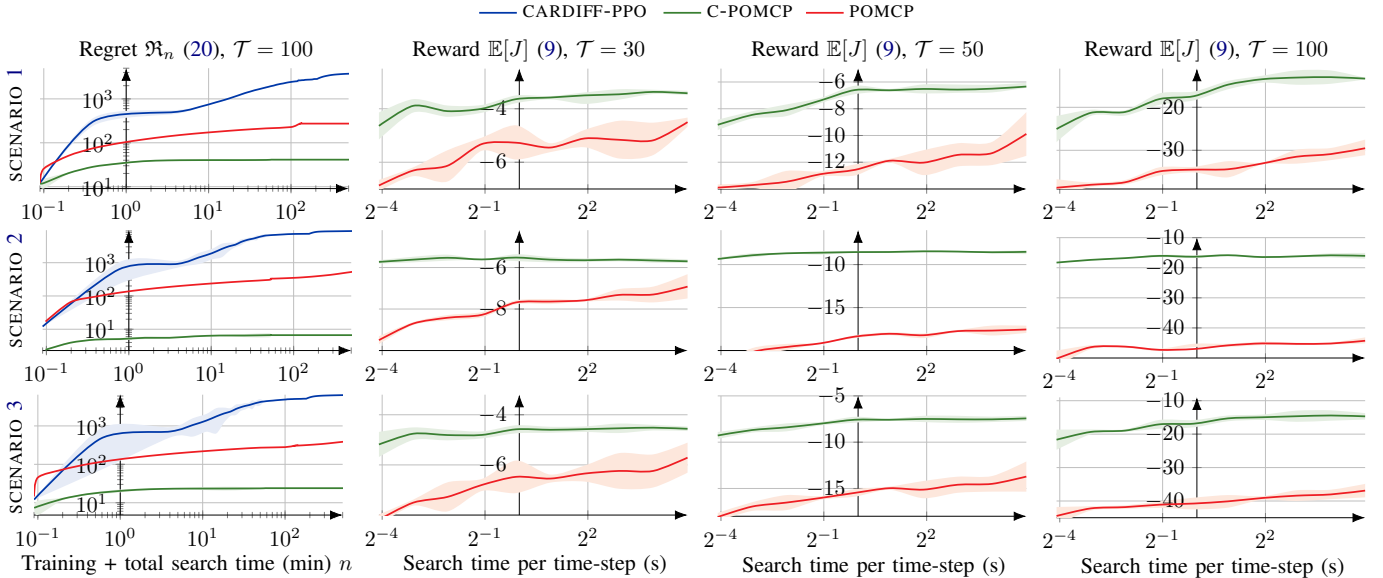


Fig. 10: Comparing C-POMCP (green curves) with baselines: CARDIFF-PPO [5] (blue curves) and POMCP [24] (red curves); rows indicate the evaluation scenario (§VII-A); the curves show the mean value from evaluations with 3 random seeds; shaded areas indicate the standard deviation; the number of data points on the x-axis is 2000 for the left-most column and 10 for the other columns.

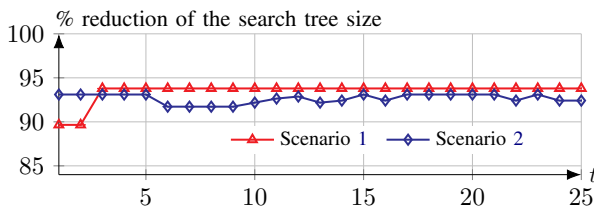


Fig. 11: Effect of the pruning of the search tree in C-POMCP.

Method	Training (min)	Search (s)	Reward $E[J]$ (9)
CARDIFF-PPO [5]	2000	10 ⁻⁴	-429 ± 167
C-POMCP	0	30	-13.32 ± 0.18
POMCP [24]	0	30	-29.51 ± 2.00

TABLE 3: Evaluation results for Scenario 4 with $\mathcal{T} = 100$.

achieved by the pruning is shown in Fig. 11. We see that the pruning reduces the size of the search tree by around 90–95%.

Lastly, Table 3 contains the results for Scenario 4. We find

that C-POMCP and POMCP are agnostic to changes in the topology within each zone. By contrast, the performance of CARDIFF-PPO reduces drastically when the topology changes, indicating that its strategy is overfitted to the training environment [5]. CARDIFF-PPO has shown similar behavior in [100].

C. Discussion of the CAGE-2 Benchmark Results

The key findings from the CAGE-2 benchmark results are:

- 1) Leveraging the causal structure of the target system, C-POMCP achieves state-of-the-art performance (Figs. 10–11, Table 2).
- 2) The interventions prescribed by C-POMCP are guaranteed to converge to optimal interventions as $s_T \rightarrow \infty$ (Thm. 4), which is consistent with the evaluation results.
- 3) C-POMCP is two orders of magnitude more efficient in computing time than the state-of-the-art method CARDIFF-PPO (Fig. 10).
- 4) C-POMCP is an online method and can adapt to changes in the topology of the target system (Table 3).

Surprisingly, the results demonstrate that C-POMCP requires only 5–15 seconds of search to achieve competitive performance on the CAGE-2 benchmark. The fact that C-POMCP performs significantly better than its non-causal version POMCP [24, Alg. 1] indicates that the main enabler of the efficiency is the causal structure, which we exploit for pruning the search space. This observation suggests limitations of existing methods that narrowly focus on *model-free* reinforcement learning and do not consider the causal structure of the underlying system.

While the results demonstrate clear benefits of C-POMCP compared to the existing methods, C-POMCP has two drawbacks. First, execution of C-POMCP is slower than that of pre-trained methods (see Table 2, typically 10^{-4} s vs 10s). Second, the performance of C-POMCP depends on the causal structure of the target system [22, Def. 2.2.1]. If no causal structure is known, the performance of C-POMCP drops (cf. the performance of C-POMCP and POMCP in Table 2).

VIII. CONCLUSION

This paper presents a formal (causal) model of CAGE-2 (M1), which is considered a standard benchmark to evaluate methods for autonomous cyber defense [4]. Based on this model, we prove the existence of optimal defender strategies (Thm. 1) and design an iterative method that converges to such a strategy (Thm. 4). The method, which we call Causal Partially Observable Monte-Carlo Planning (C-POMCP), leverages causal structure to prune, construct and traverse a search tree (Alg. 1). C-POMCP has four advantages over the state-of-the-art methods that have been proposed in the context of CAGE-2: (i) it is two orders of magnitude more computationally efficient (Fig. 10); (ii) it achieves better performance (Table. 2); (iii) it is an online method which adapts to topology changes in the target system (Table 3); and (iv), it produces provably optimal defender strategies (Thm. 4). Future work will focus on leveraging causal discovery techniques to automate the process of creating a causal graph of the underlying system.

IX. ACKNOWLEDGMENTS

The authors are grateful to DARPA and program manager Tejas Patel for supporting this research. The authors would also like to thank the Siemens research team for discussions and feedback: Enrico Lovat, Jagannadh Vempati, Anton Kocheturov, Arun Ramamurthy, Arif Haque, and Abhishek Ramchandran. Finally, the authors thank KTH researchers Forough Shahab Samani, Xiaoxuan Wang, and Duc Huy Le for constructive comments.

APPENDIX A PROOF OF THEOREM 3

1) CASE: $t = 1$.

PROOF: \mathbf{b}_1 is given, hence $\hat{\mathbf{b}}_1 = \mathbf{b}_1$.

2) CASE: $t > 1$.

PROOF: Assume $\hat{\mathbf{b}}_{t-1} = \mathbf{b}_{t-1}$ and let

$$g(\bar{\sigma}_t) \triangleq \sum_{\sigma_{t-1}} \hat{\mathbf{b}}_{t-1}(\sigma_{t-1}) P(\bar{\sigma} | \sigma_{t-1}, \text{do}(\hat{\mathbf{X}}_{t-1} = \hat{\mathbf{x}}_{t-1})).$$

We then have that

$$\begin{aligned} \mathbf{b}_t(\sigma) &= \mathbb{E}_{\bar{\sigma} \sim \mathbf{b}_t} [\mathbb{1}_{\sigma=\bar{\sigma}}] = \sum_{\bar{\sigma}} \mathbf{b}_t(\bar{\sigma}) \mathbb{1}_{\sigma=\bar{\sigma}} \\ &\stackrel{(a)}{=} \sum_{\bar{\sigma}} \frac{g(\bar{\sigma})}{g(\bar{\sigma})} \mathbf{b}_t(\bar{\sigma}) \mathbb{1}_{\sigma=\bar{\sigma}} = \mathbb{E}_{\bar{\sigma} \sim g} \left[\frac{\mathbf{b}_t(\bar{\sigma})}{g(\bar{\sigma})} \mathbb{1}_{\sigma=\bar{\sigma}} \right] \\ &\stackrel{(b)}{=} \mathbb{E}_{\bar{\sigma} \sim g} \left[\frac{\eta P(\mathbf{o}_t | \sigma_t) g(\bar{\sigma})}{g(\bar{\sigma})} \mathbb{1}_{\sigma=\bar{\sigma}} \right] \\ &= \mathbb{E}_{\bar{\sigma} \sim g} [\eta P(\mathbf{o}_t | \sigma_t) \mathbb{1}_{\sigma=\bar{\sigma}}], \end{aligned} \quad (21)$$

where (b) follows from the definition of \mathbf{b} .

As $\hat{\mathbf{b}}_{t-1} = \mathbf{b}_{t-1}$, the denominator in (a) is non-zero for all $\bar{\sigma}$ where $\mathbf{b}_t(\bar{\sigma}) > 0$. Since the particles are distributed according to $\eta' \eta P(\mathbf{o}_t | \sigma_t) g(\bar{\sigma}_t)$ (η' is a normalizing factor), it follows from the strong law of large numbers [101, Thm. 6.2] that $\hat{\mathbf{b}}(\sigma_t) = \frac{1}{M} \sum_{i=1}^M \mathbb{1}_{\sigma_t=\hat{\sigma}_t^{(i)}}$ converges P -almost surely to (21) as $M \rightarrow \infty$. (Remark: the probability measure P in (21) exists since $|\text{dom}(\Sigma_t) \cup \text{dom}(\mathbf{O}_t)| < \infty$ (Thm. 1, [102, Thm. 2.2.1]).) \square

APPENDIX B PROOF OF THEOREM 4

It follows from Thm. 3 and [24, Lem. 1–2] that C-POMCP corresponds to the UCT algorithm [98, Fig. 1] when $M \rightarrow \infty$. Hence, we can base the proof of convergence of C-POMCP on the proof of convergence for UCT, which was originally published in [98]. The key insight behind the proof is that the decision problem at each node in the search tree corresponds to a non-stationary multi-armed bandit (MAB), which becomes stationary if the prescribed actions at the child nodes converge. Further, the tree policy corresponds to the UCB1 algorithm [103, Fig. 1]. As a consequence, it suffices to prove that UCB1 converges at each node in the search tree. Towards this proof, we state and prove the following six lemmas.

Notation. $K = \mathcal{O}(|2\mathbf{X}_t|)$ is the number of arms in the MAB at each node in the search tree; t indexes the MAB rounds; $R_{i,t}$ is the reward of arm i at round t ; $\bar{R}_{i,n} = \frac{1}{n} \sum_{k=1}^n R_{i,k}$ is the mean reward of arm i based on n samples; $\mu_{i,n}$ is the mean of $\bar{R}_{i,n}$; $\mu_i \triangleq \lim_{n \rightarrow \infty} \mu_{i,n}$; $\mu_i \triangleq \mu_{i,n} - \delta_{i,n}$; $T_i(t)$ is the number of times arm i has been pulled at round t ; $\Delta_i \triangleq \mu^* - \mu_i$; I_t is the arm picked at round t ; and $c_{t,n}$ is the exploration term in UCB1 for an arm that has been pulled n times at round t . Quantities related to the optimal arm are superscripted by $*$, i.e., μ^* , $T^*(t)$, etc.

Assumption 1 (Bounded rewards and asymptotic stationarity).

- 1) $R_{i,n} \in [0, 1]$ for all i and n .
- 2) The limit $\mu_i = \lim_{t \rightarrow \infty} \mu_{i,t}$ exists for each arm i .
- 3) There exists a constant C_p and an integer N_p such that for $n \geq N_p$ and any $\delta \geq 0$, the following bounds hold.

$$P(n\bar{R}_{i,n} \geq n\mu_{i,n} + C_p \sqrt{n \ln(1/\delta)}) \leq \delta$$

$$P(n\bar{R}_{i,n} \geq n\mu_{i,n} - C_p \sqrt{n \ln(1/\delta)}) \leq \delta.$$

Lemma 1. Given Assumption 1, if $c_{t,n} = 2C_p \sqrt{\frac{\ln t}{n}}$, then

$$P(\bar{R}_{i,n} \geq \mu_{i,n} + c_{t,n}) \leq t^{-4} \quad n \geq N_p$$

$$P(\bar{R}_{i,n} \geq \mu_{i,n} - c_{t,n}) \leq t^{-4} \quad n \geq N_p.$$

Proof.

$$\begin{aligned} P(n\bar{R}_{i,n} \geq n\mu_{i,n} + C_p\sqrt{n\ln(1/\delta)}) &\stackrel{\text{(Assumption 1)}}{\leq} \delta \\ \implies P(\bar{R}_{i,n} \geq \mu_{i,n} + C_p\sqrt{\frac{\ln(1/\delta)}{n}}) &\geq \delta \\ \stackrel{\delta=t^{-4}}{\implies} P(\bar{R}_{i,n} \geq \mu_{i,n} + 2C_p\sqrt{\frac{\ln(t)}{n}}) &\geq t^{-4}. \end{aligned}$$

□

Lemma 2. If Assumption 1 holds, then there exists an integer $N_0(\epsilon)$ such that $t \geq N_0(\epsilon) \implies |\delta_{i,t}| \leq \frac{\epsilon\Delta_i}{2}$ and $|\delta_{j^*,t}| \leq \min_i \frac{\epsilon\Delta_i}{2}$ for all $\epsilon > 0$.

Proof. Follows by the definition of Assumption 1. □

Lemma 3. Given Assumption 1, if the exploration term used by UCB1 [103, Fig. 1] is $c_{t,s} = 2C_p\sqrt{\frac{\ln t}{s}}$, then

$$\mathbb{E}[T_i(t)] \leq \frac{16C_p^2 \ln t}{(1-\epsilon)^2 \Delta_i^2} + N_0(\epsilon) + N_p + 1 + \frac{\pi^2}{3} \quad (22)$$

for all $\epsilon > 0$ and each sub-optimal arm i .

Proof. Let $A_0(t, \epsilon) \triangleq \min\{s | c_{t,s} \leq (1-\epsilon)\Delta_i/2\}$ and $A(t, \epsilon) \triangleq \max[A_0(t, \epsilon), N_0(\epsilon), N_p]$. Next note that

$$\begin{aligned} c_{t,s} \leq (1-\epsilon)\Delta_i/2 &\implies 2C_p\sqrt{\frac{\ln t}{s}} \leq (1-\epsilon)\Delta_i/2 \\ \implies 16C_p\frac{\ln t}{s} \leq (1-\epsilon)^2\Delta_i^2 &\implies s \geq \frac{16C_p \ln t}{(1-\epsilon)^2\Delta_i^2} \\ \implies A_0(t, \epsilon) &= \left\lceil \frac{16C_p \ln t}{(1-\epsilon)^2\Delta_i^2} \right\rceil. \end{aligned}$$

Now consider $T_i(n)$. By definition:

$$\begin{aligned} T_i(n) &= 1 + \sum_{t=K+1}^n \mathbb{1}\{I_t = i\} \\ &= 1 + \sum_{t=K+1}^n \mathbb{1}\{I_t = i, T_i(t-1) \geq A(n, \epsilon)\} + \\ &\quad \sum_{t=K+1}^n \mathbb{1}\{I_t = i, T_i(t-1) < A(n, \epsilon)\} \\ &\stackrel{(a)}{\leq} A(n, \epsilon) + \sum_{t=K+1}^n \mathbb{1}\{I_t = i, T_i(t-1) \geq A(n, \epsilon)\} \\ &\stackrel{(b)}{\leq} A(n, \epsilon) + \sum_{t=K+1}^n \mathbb{1}\left\{\bar{R}_{T^*(t-1)}^* + c_{t-1, T^*(t-1)} \leq \bar{R}_{i, T_i(t-1)} + c_{t-1, T_i(t-1)}, T_i(t-1) \geq A(n, \epsilon)\right\} \\ &\leq A(n, \epsilon) + \sum_{t=K+1}^n \mathbb{1}\left\{\min_{0 \leq s \leq t} \bar{R}_s^* + c_{t-1, s} \leq \max_{A(n, \epsilon) < s_i < t} \bar{R}_{i, s_i} + c_{t-1, s_i}\right\} \\ &\leq A(n, \epsilon) + \sum_{t=K+1}^n \sum_{s=1}^{t-1} \sum_{s_i=A(n, \epsilon)}^{t-1} \mathbb{1}\left\{\bar{R}_s^* + c_{t-1, s} \leq \bar{R}_{i, s_i} + c_{t-1, s_i}\right\} \end{aligned} \quad (23)$$

$$\leq \bar{R}_{i, s_i} + c_{t-1, s_i}\},$$

where (a) follows because the second sum is upper bounded by $n-K$ and $n < A(n, \epsilon) \implies T_i(n) < A(n, \epsilon)$. (b) follows from the arm-selection rule in UCB1 [103, Fig. 1].

Next note that for $t \geq A(n, \epsilon) \geq N_0(\epsilon)$, we have $\mu_t^* \geq \mu_{i,t} + 2c_{t,s_i}$. This inequality holds because

$$\begin{aligned} \mu_t^* \geq \mu_{i,t} + 2c_{t,s_i} &\iff \mu_t^* - \mu_{i,t} - 4C_p\sqrt{\frac{\ln t}{s_i}} \geq 0 \\ \stackrel{t \geq A_0(n, \epsilon)}{\iff} \mu_t^* - \mu_{i,t} - (1-\epsilon)\Delta_i &\geq 0 \\ \stackrel{\text{Lemma 2}}{\iff} \mu_t^* + \delta^* - \mu_{i,t} - \delta_{i,t} - (1-\epsilon)\Delta_i &\geq 0 \\ \stackrel{\text{Lemma 2}}{\iff} \mu_t^* - \epsilon\Delta_i - \mu_{i,t} - (1-\epsilon)\Delta_i &\geq 0 \\ \iff \mu_t^* - \mu_{i,t} - \Delta_i &\geq 0 \iff \Delta_i - \Delta_i \geq 0. \end{aligned} \quad (24)$$

Using the above inequality, we deduce that

$$\begin{aligned} P(\bar{R}_s^* + c_{t-1,s} \leq \bar{R}_{i,s_i} + c_{t-1,s_i}) &\leq \\ P(\bar{R}_s^* \leq \mu_t^* + c_{t,s}) + P(\bar{X}_{i,s_i} \geq \mu_{i,t} + c_{t,s_i}) &. \end{aligned} \quad (25)$$

This follows because if the left inequality above holds and the right inequalities do not hold, we obtain

$$\begin{aligned} \bar{R}_s^* + c_{t-1,s} &\leq \bar{R}_{i,s_i} + c_{t-1,s_i} \\ \implies \mu_t^* - c_{t,s} + c_{t-1,s} &< \mu_{i,t} + c_{t,s_i} + c_{t-1,s_i} \\ \implies \mu_t^* &< \mu_{i,t} + 2c_{t,s_i}, \end{aligned}$$

which by (24) is false for $t \geq A(n, \epsilon) \geq N_0(\epsilon)$. Now we take expectations of both sides of the inequality in (23) and plug in (25), which gives

$$\begin{aligned} \mathbb{E}[T_i(n)] &\leq A(n, \epsilon) + \sum_{t=K+1}^n \sum_{s=1}^{t-1} \sum_{s_i=A(n, \epsilon)}^{t-1} P(\bar{R}_s^* \leq \mu_t^* + c_{t,s}) \\ &\quad + P(\bar{X}_{i,s_i} \geq \mu_{i,t} + c_{t,s_i}) \\ &\stackrel{\text{(Lemma 1)}}{\leq} A(n, \epsilon) + \sum_{t=K+1}^n \sum_{s=1}^{t-1} \sum_{s_i=A(n, \epsilon)}^{t-1} 2t^{-4} \\ &\leq A(n, \epsilon) + \sum_{t=1}^{\infty} \sum_{s=1}^t \sum_{s_i=1}^t 2t^{-4} \\ &= A(n, \epsilon) + \sum_{t=1}^{\infty} t^{-2} + t^{-3} \leq A(n, \epsilon) + \sum_{t=1}^{\infty} t^{-2} + \sum_{t=1}^{\infty} t^{-2} \\ &\stackrel{(a)}{=} A(n, \epsilon) + \frac{\pi^2}{3} \leq \frac{16C_p \ln t}{(1-\epsilon)^2 \Delta_i^2} + 1 + N_0(\epsilon) + N_p + \frac{\pi^2}{3}, \end{aligned}$$

where (a) follows from the Riemann zeta function $\zeta(2) = \sum_{t=1}^{\infty} t^{-2} = \frac{\pi^2}{6}$. □

Lemma 4 (Lower bound). Given Assumption 1, there exists a positive constant ρ such that for all i and t , $T_i(t) \geq \lceil \rho \log t \rceil$.

Proof. Since $R_{i,t} \in [0, 1]$ and $T_i(t-1) \geq 1$ for all $t \geq K$, there exists a constant M such that

$$\begin{aligned} \mu_{i,t} + 2C_p\sqrt{\frac{\ln t}{T_i(t-1)}} &\leq M \\ \implies T_i(t-1) &\geq \frac{4C_p^2 \ln t}{(M - \mu_{i,t} - \delta_{i,t})^2} \end{aligned}$$

for all i and $K \leq t < \infty$. Next note that Assumption 1 implies that $\lim_{t \rightarrow \infty} \delta_{i,t} = 0$, which means that there exists a constant $\rho \geq \frac{4C_p^2}{(M - \mu_i - \delta_{i,t})^2}$. Hence $T_i(t) \geq \lceil \rho \log t \rceil$. \square

Lemma 5. Let $\bar{R}_n = \sum_{i=1}^K \frac{T_i(n)}{n} \bar{X}_{i,T_i(n)}$ and $N_0 = N_0(\epsilon = \frac{1}{2})$. Then, the following holds under Assumption 1.

$$|\mathbb{E}[\bar{R}_n] - \mu^*| \leq |\delta_n^*| + \mathcal{O}\left(\frac{K(C_p^2 \ln n + N_0)}{n}\right).$$

Proof. By the triangle inequality,

$$\begin{aligned} |\mathbb{E}[\bar{R}_n] - \mu^*| &\leq |\mu^* - \mu_n^*| + |\mu_n^* - \mathbb{E}[\bar{R}_n]| \\ &= |\delta_n^*| + |\mu^* - \mathbb{E}[\bar{X}_n]|. \end{aligned}$$

Hence it only remains to bound $|\mu^* - \mathbb{E}[\bar{X}_n]|$. By definition:

$$\begin{aligned} |\mu^* - \mathbb{E}[\bar{X}_n]| &= \left| \mu^* - \mathbb{E} \left[\sum_{i=1}^K \frac{T_i(n) \bar{R}_{i,T_i(n)}}{n} \right] \right| \quad (26) \\ \implies n |\mu^* - \mathbb{E}[\bar{X}_n]| &= \left| \sum_{t=1}^n \mathbb{E}[R_t^*] - \mathbb{E} \left[\sum_{i=1}^K T_i(n) \bar{R}_{i,T_i(n)} \right] \right| \\ &\stackrel{(a)}{=} \left| \sum_{t=1}^n \mathbb{E}[R_t^*] - \mathbb{E} \left[T^*(n) \bar{R}_{T^*(n)}^* \right] \right| - \mathbb{E} \left[\sum_{i \neq i^*} T_i(n) \bar{R}_{i,T_i(n)} \right], \end{aligned}$$

where (a) follows because $\bar{R}_{i,t} \in [0, 1]$ for all i and t (Assumption 1). We start by bounding the second term in (26):

$$\begin{aligned} \mathbb{E} \left[\sum_{i \neq i^*} T_i(n) \bar{R}_{i,T_i(n)} \right] &\leq \mathbb{E} \left[\sum_{i \neq i^*} T_i(n) \right] \\ &\stackrel{\text{(Lemma 3)}}{\leq} K \left(\frac{16C_p^2 \ln t}{(1-\epsilon)^2 \Delta_i^2} + N_0(\epsilon) + N_p + 1 + \frac{\pi^2}{3} \right) \\ &= \mathcal{O}(K(C_p^2 \ln n + N_0(\epsilon))). \end{aligned}$$

Now we consider the first term in (26). Note that $T^*(n) \bar{R}_{T^*(n)}^* = \frac{T^*(n)}{T^*(n)} \sum_{t=1}^{T^*(n)} \bar{R}_t^* = \sum_{t=1}^{T^*(n)} \bar{R}_t^*$. Using this expression we obtain:

$$\begin{aligned} \left| \sum_{t=1}^n \mathbb{E}[R_t^*] - \mathbb{E} \left[T^*(n) \bar{R}_{T^*(n)}^* \right] \right| &= \left| \mathbb{E} \left[\sum_{t=1}^n R_t^* - \sum_{t=1}^{T^*(n)} R_t^* \right] \right| \\ &\stackrel{(a)}{=} \sum_{t=T^*(n)+1}^n \mathbb{E}[R_t^*] \leq \mathbb{E}[n - T^*(n)] = \sum_{i \neq i^*} \mathbb{E}[T_i(n)] \\ &\stackrel{\text{(Lemma 3)}}{\leq} K \left(\frac{16C_p^2 \ln t}{(1-\epsilon)^2 \Delta_i^2} + N_0(\epsilon) + N_p + 1 + \frac{\pi^2}{3} \right) \\ &= \mathcal{O}(K(C_p^2 \ln n + N_0(\epsilon))), \end{aligned}$$

where (a) follows from the fact that $\bar{R}_{i,t} \in [0, 1]$ for all i and t (Assumption 1). \square

Lemma 6. Let n_0 be such that $\sqrt{n_0} \geq \mathcal{O}(K(C_p^2 \ln n_0 + N_0(\frac{1}{2})))$. Given Assumption 1, the following holds for any $n \geq n_0$ and $\delta > 0$:

$$P \left(n \bar{X}_n \geq n \mathbb{E}[\bar{X}_n] + 9\sqrt{2 \ln(2/\delta)} \right) \leq \delta$$

$$P \left(n \bar{X}_n \geq n \mathbb{E}[\bar{X}_n] - 9\sqrt{2 \ln(2/\delta)} \right) \leq \delta.$$

Proof. This lemma was originally proved by Kocsis & Szepesvári [98, Thm. 5]. A more accessible version of the proof can be found in [104, Thm. 5]. We omit the full proof for brevity. For the sake of completeness, we briefly outline the main ideas behind the proof here. The proof involves defining a counting process that represents the number of times a sub-optimal arm is pulled and then bounding the deviation of this process. Key to this argument is the Hoeffding-Azuma inequality [98, Lem. 8–10]. By leveraging this inequality and martingale theory, it is possible to conclude that the desired inequalities must hold. \square

Lemma 7. Given Assumption 1, $\lim_{t \rightarrow \infty} P(I_t \neq i^*) = 0$.

Proof. Let $p_{i,t} = P(\bar{R}_{i,T_i(t)} \geq \bar{R}_{T^*(t)}^*)$. Clearly, $P(I_t \neq i^*) \leq \sum_{i \neq i^*} p_{i,t}$. Hence it suffices to show that $p_{i,t} \leq \frac{\epsilon}{K}$ for all i and any $\epsilon > 0$. Towards this proof, note that if $\bar{R}_{i,T_i(t)} < \mu_i + \frac{\Delta_i}{2}$ and $\bar{R}_{T^*(t)}^* > \mu^* - \frac{\Delta}{2}$, then

$$\bar{R}_{i,T_i(t)} < \mu_i + \frac{\Delta_i}{2} = \mu^* - \frac{\Delta_i}{2} < \bar{R}_{T^*(t)}^*.$$

As a consequence,

$$p_{i,t} \leq P \left(\bar{R}_{i,T_i(t)} < \mu_i + \frac{\Delta_i}{2} \right) + P \left(\bar{R}_{T^*(t)}^* > \mu^* - \frac{\Delta}{2} \right).$$

Since $T_i(t)$ grows slower than $T^*(t)$, it suffices to bound the first of the two terms above. By definition:

$$\begin{aligned} &P \left(\bar{R}_{i,T_i(t)} < \mu_i + \frac{\Delta_i}{2} \right) \\ &= P \left(\bar{R}_{i,T_i(t)} < \mu_{i,T_i(t)} - |\delta_{i,T_i(t)}| + \frac{\Delta_i}{2} \right). \end{aligned}$$

Next note that $|\delta_{i,T_i(t)}|$ converges to 0 by Assumption 1. Hence, we can assume that $|\delta_{i,T_i(t)}|$ is decreasing in t without loss of generality. It then follows from Lemma 4 that $|\delta_{i,T_i(t)}| \leq |\delta_{i,\lceil \rho \log t \rceil}|$. Now consider $t \geq \lceil \rho \log t \rceil \geq N_0(\frac{\Delta}{4})$, then $|\delta_{i,T_i(t)}| \leq |\delta_{i,\lceil \rho \log t \rceil}| \leq \frac{\Delta_i}{4}$ by Lemma 2. As a consequence,

$$\begin{aligned} &P \left(\bar{R}_{i,T_i(t)} < \mu_{i,T_i(t)} - |\delta_{i,T_i(t)}| + \frac{\Delta_i}{2} \right) \quad (27) \\ &\leq P \left(\bar{R}_{i,T_i(t)} < \mu_{i,T_i(t)} + \frac{\Delta_i}{4} \right) \\ &\leq P \left(\bar{R}_{i,T_i(t)} < \mu_{i,T_i(t)} + \frac{\Delta_i}{4}, T_i(t) \geq a \right) + P(T_i(t) \leq a). \end{aligned}$$

Since $\lim_{t \rightarrow \infty} T_i(t) = \infty$ (Lemma 4), we have that $\lim_{t \rightarrow \infty} P(T_i(t) < a) = 0$ for any a . Hence it suffices to bound the first term in (27), which can be done as follows.

$$\begin{aligned} &P \left(\bar{R}_{i,T_i(t)} < \mu_{i,T_i(t)} + \frac{\Delta_i}{4}, T_i(t) \geq a \right) \leq \\ &P \left(\bar{R}_{i,T_i(t)} < \mu_{i,T_i(t)} + \frac{\Delta_i}{4} \mid T_i(t) \in [a, b] \right) P(T_i(t) \in [a, b]) \\ &+ P(T_i(t) \notin [a, b]). \end{aligned}$$

Next note that

$$P \left(\bar{R}_{i,T_i(t)} < \mu_{i,T_i(t)} + \frac{\Delta_i}{4} \mid T_i(t) \in [a, b] \right)$$

$$\begin{aligned} &\leq \sum_{k=a}^b P\left(\bar{R}_{i,k} < \mu_{i,k} + \frac{\Delta_i}{4}\right) \\ &\leq (b-a+1) \max_{a \leq k \leq b} P\left(\bar{R}_{i,k} < \mu_{i,k} + \frac{\Delta_i}{4}\right). \end{aligned}$$

Now we use Assumption 1, which implies that the value of a in the expression above can be chosen such that for all $t \geq a$, $(t+1)P(\bar{X}_{i,t} \geq \mu_{i,t} + \frac{\Delta_i}{4}) < \frac{\epsilon}{2K}$, which means that

$$\begin{aligned} &(b-a+1) \max_{a \leq k \leq b} P\left(\bar{R}_{i,k} < \mu_{i,k} + \frac{\Delta_i}{4}\right) \\ &=^{b=2a} (a+1) \max_{a \leq k \leq b} P\left(\bar{R}_{i,k} < \mu_{i,k} + \frac{\Delta_i}{4}\right) \\ &\leq (a+1)P\left(\bar{R}_{i,a} < \mu_{i,a} + \frac{\Delta_i}{4}\right) \leq \frac{\epsilon}{2K}. \end{aligned}$$

Putting the bounds above together, we get:

$$P(I_t \neq i^*) \leq \sum_{i \neq i^*} p_{it} \leq K \frac{\epsilon}{K} = \epsilon.$$

□

Now we use Lemmas 1–7 to prove Thm. 3.

A. Proof of Theorem 4

The proof uses mathematical induction on the time horizon \mathcal{T} , corresponding to the search tree's depth. Without loss of generality, we assume that the target variables are normalized to the interval $[0, 1]$.

For the inductive base case where $\mathcal{T} = 2$, C-POMCP corresponds to a stationary MAB problem, which means that Assumption 1.1–2 hold. Further, Assumption 1.3 follows from Hoeffding's inequality:

$$P\left(\bar{R}_{i,n} \leq \mu_{i,n} \pm \frac{1}{n} \sqrt{\frac{\ln t}{n}}\right) \leq e^{-2\frac{\sqrt{\frac{2 \ln t}{n}}}{n}} = e^{-4 \ln t} = t^{-4}.$$

As a consequence, we can invoke Lemma 5 and Lemma 7, which asserts that the theorem statement holds when $\mathcal{T} = 2$.

Assume by induction that the theorem statement holds for time horizons $3, 4, \dots, \mathcal{T}-1$ and consider time horizon \mathcal{T} . By Thm. 3, the problem of finding an optimal intervention from the root node when the horizon is \mathcal{T} corresponds to a non-stationary MAB with correlated rewards. This MAB satisfies Assumption 1.1 if the rewards are divided by \mathcal{T} . Further, it follows from the induction hypothesis that the reward distributions in each subtree converge, which means that Assumption 1.2 holds. Moreover, the induction hypothesis together with Lemma 6 implies that Assumption 1.3 is satisfied. As a consequence, we can apply Lemma 7, which ensures that the intervention prescribed at the root converges to an optimal intervention. Similarly, we can apply Lemma 5, which states that

$$|\mathbb{E}[\bar{R}_n - \mu_n^*]| \leq |\delta^*| + \mathcal{O}\left(\frac{KC_p^2 \ln n + N_0}{n}\right),$$

where \bar{R}_n is the average reward at the root. By the induction hypothesis,

$$|\delta^*| = \mathcal{O}\left(\frac{K(\mathcal{T}-1) \log n + K^{\mathcal{T}-1}}{n}\right).$$

Parameters	Values
Model parameters	
$\beta_{R,1}, \beta_{R,2}, \beta_{R,3}$	0.1, 1, 1
$\beta_{i,t,z}$	0 if $I_{i,t} \neq R$
q_t	1 for restore interventions, 0 otherwise
ψ_{z_i}	10 if $z_i = 3$, 0 otherwise
Cyborg version [105]	commit 9421c8e
C-POMCP and POMCP [24, Alg. 1]	
search time, default node value	0.05s–30s, 0
M, γ, c	1000, 0.99, 0.5
rollout depth, maximum search depth	4, 50
intervention space	intervention space described in [5]
base strategy, base value	$\hat{\pi}_D(\text{do}(\emptyset)) = 1, J_{\hat{\pi}}(\cdot) = 0$
CARDIFF-PPO [81, Alg. 1] [5]	
learning rate, # hidden layers,	$5148 \cdot 10^{-5}, 1$
# neurons per layer, # steps between updates,	64, 2048,
batch size, discount factor γ	16, 0.99
GAE λ , clip range, entropy coefficient	0.95, 0.2, $2 \cdot 10^{-4}$
value coefficient, max gradient norm	0.102, 0.5
feature representation	the original cyborg features [105] & one-hot encoded scan-state & decoy-state for each node

TABLE 4: Hyperparameters.

Hence,

$$\begin{aligned} |\mathbb{E}[\bar{R}_n - \mu_n^*]| &\leq \mathcal{O}\left(\frac{K(\mathcal{T}-1) \log n + K^{\mathcal{T}-1}}{n}\right) \\ &\quad + \mathcal{O}\left(\frac{KC_p^2 \ln n + N_0}{n}\right). \end{aligned}$$

Thus, it only remains to bound N_0 . It follows from Lemma 2 that N_0 is upper bounded by the smallest value of n for which the following inequality holds

$$\begin{aligned} \frac{K(\mathcal{T}-1) \log n + K^{\mathcal{T}-1}}{n} &\geq \frac{\Delta_i}{2} \\ \implies \frac{2(K^{\mathcal{T}-1} + K(\mathcal{T}-1) \log n)}{\Delta_i} &\geq n \\ \implies N_0 &= \mathcal{O}(K^{\mathcal{T}-1}). \end{aligned}$$

As a consequence,

$$\begin{aligned} |\mathbb{E}[\bar{R}_n - \mu_n^*]| &\leq \mathcal{O}\left(\frac{K(\mathcal{T}-1) \log n + K^{\mathcal{T}-1}}{n}\right) \\ &\quad + \mathcal{O}\left(\frac{KC_p^2 \ln n + K^{\mathcal{T}}}{n}\right) = \mathcal{O}\left(\frac{(K\mathcal{T} \log n + K^{\mathcal{T}})}{n}\right). \end{aligned}$$

Hence, by induction, the theorem holds for all \mathcal{T} . □

APPENDIX C HYPERPARAMETERS

The hyperparameters used for the evaluation are listed in Table 4 and were obtained through random search.

APPENDIX D CONFIGURATION OF THE TARGET SYSTEM (FIG. 1)

The configuration of the target system in CAGE-2 (Fig. 1) is available in Table 5. The attacker actions are listed in Table 6 and the defender interventions are listed in Table 7. The decoy services are listed in Table 8, and the workflow graph is shown in Fig. 12.

Node ID, hostname	Processes	Ports	Users	Vulnerabilities
1, CLIENT-1	SSHD.EXE FEMITTER.EXE	22 21	SSHD_SERVER SYSTEM	CWE-251 CVE-2020-26299
2, CLIENT-2	SMSS.EXE SVCHOST.EXE SVCHOST.EXE	445,139 135 3389	SYSTEM SYSTEM NETWORK	- - CVE-2019-0708
3, CLIENT-3	MYSQL APACHE2 SMTP	3389 80,443 25	ROOT WWW-DATA ROOT	CVE-2019-0708 CWE-89, HTTP-(S)RFI CVE-2016-1000282
4, CLIENT-4	SSHD MYSQL APACHE2 SMTP	22 3390 80, 443 25	ROOT ROOT WWW-DATA ROOT	CWE-251 CWE-89 CWE-89, HTTP-(S)RFI CVE-2016-1000282
5, ENTERPRISE-1	SSHD.EXE	22	ROOT	CWE-251
6, ENTERPRISE-2	SSHD.EXE SVCHOST.EXE SVCHOST.EXE SMSS.EXE TOMCAT8.EXE	22 135 3389 445,139 80,443	SSHD_SERVER SYSTEM SYSTEM SYSTEM NETWORK	CWE-251 - CVE-2019-0708 CVE-2017-0144 CWE-89,HTTP-(S)RFI
7, ENTERPRISE-3	SSHD.EXE SVCHOST.EXE SVCHOST.EXE SMSS.EXE TOMCAT8.EXE	22 135 3389 445,139 80,443	SSHD_SERVER SYSTEM SYSTEM SYSTEM NETWORK	CWE-251 - CVE-2019-0708 CVE-2017-0144 CWE-89,HTTP-(S)RFI
8, OPERATIONAL-1	SSHD	22	ROOT	CWE-251
9, OPERATIONAL-2	SSHD	22	ROOT	CWE-251
10, OPERATIONAL-3	SSHD	22	ROOT	CWE-251
11, OPERATIONAL-4	SSHD	22	ROOT	CWE-251
12, DEFENDER	SSHD SYSTEMD	22 53,78	ROOT SYSTEMD+	CWE-251
13, ATTACKER	SSHD.EXE FEMITTER.EXE	22 21	SSHD_SERVER SYSTEM	CWE-251 CVE-2020-26299

TABLE 5: Configuration of the target system in CAGE-2 (Fig. 1); vulnerabilities are identified by their identifiers in the Common Vulnerabilities and Exposures (CVE) database [106] and the Common Weakness Enumeration (CWE) list [107].

Type	Actions	MITRE ATT&CK technique
Reconnaissance	Subnet scan for nodes Port scan on a specific node	T1018 system discovery T1046 service scanning
Exploits	CVE-2017-0144, HTTP-SRFI SQL INJECTION (CWE-89) CVE-2016-1000282 CVE-2020-26299 HTTP-RFI	T1210 service exploitation T1210 service exploitation T1210 service exploitation T1210 service exploitation
Brute-force	SSH	T1110 brute force
Escalate	Escalate privileges of user to root	T1068 privilege escalation
Impact	Stop services running on node	T1489 service stop

TABLE 6: Attacker actions in CAGE-2 [4].

ID	Name	Description
1	DECOY-APACHE	Starts a vulnerable APACHE HTTP server decoy
2	DECOY-FEMITTER	Starts a vulnerable FEMITTER FTP server decoy
3	DECOY-SMTP	Starts a vulnerable HARAKA SMTP server decoy
4	DECOY-SMSS	Starts a vulnerable SMSS server decoy
5	DECOY-SSHD	Starts an SSH server decoy with a weak password
6	DECOY-SVCHOST	Starts a vulnerable SVCHOST.EXE process decoy
7	DECOY-TOMCAT	Starts a vulnerable TOMCAT HTTP server decoy
8	DECOY-VSFTPD	Starts a vulnerable VSFTPD FTP server decoy

TABLE 8: Decoy services in CAGE-2 [4].

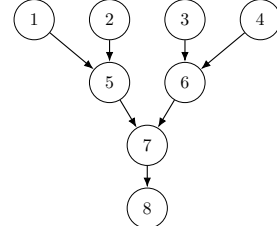


Fig. 12: Workflow graph \mathcal{G}_W in CAGE-2 [4]; circles represent nodes of the target system (Fig. 1) and edges represent service dependencies.

REFERENCES

- [1] T. Alpcan and T. Basar, *Network Security: A Decision and Game-Theoretic Approach*, 1st ed. USA: Cambridge University Press, 2010.
- [2] E. Miehling, M. Rasouli, and D. Tenekezis, *Control-Theoretic Approaches to Cyber-Security*. Springer, 2019, pp. 12–28.
- [3] Y. Huang, L. Huang, and Q. Zhu, “Reinforcement learning for feedback-enabled cyber resilience,” *Annual Reviews in Control*, 2022.
- [4] CAGE, “Ttcp cage challenge 2,” in *AAAI-22 Workshop on Artificial Intelligence for Cyber Security (AICS)*, 2022, <https://github.com/cage-challenge/cage-challenge-2>.
- [5] S. Vyas, J. Hannay, A. Bolton, and P. P. Burnap, “Automated cyber defence: A review,” 2023, code: <https://github.com/john-cardiff/cyborg-cage-2>.
- [6] M. Wolk, A. Applebaum, C. Dennler, P. Dwyer, M. Moskowitz, H. Nguyen, N. Nichols, N. Park, P. Rachwalski, F. Rau, and A. Webster, “Beyond cage: Investigating generalization of learned autonomous network defense policies,” 2022.
- [7] E. Bates, V. Mavroudis, and C. Hicks, “Reward shaping for happier autonomous cyber security agents,” in *Proceedings of the 16th ACM Workshop on Artificial Intelligence and Security*, ser. AISec ’23, New York, NY, USA, 2023, p. 221–232.
- [8] M. Foley, C. Hicks, K. Highnam, and V. Mavroudis, “Autonomous network defence using reinforcement learning,” in *Proceedings of the 2022 ACM on Asia Conference on Computer and Communications Security*, ser. ASIA CCS ’22. New York, NY, USA: Association for Computing Machinery, 2022, p. 1252–1254.
- [9] M. Foley, M. Wang, Z. M. C. Hicks, and V. Mavroudis, “Inroads into autonomous network defence using explained reinforcement learning,” 2023, <https://arxiv.org/abs/2306.09318>.
- [10] K. Heckel, “Neuroevolution for autonomous cyber defense,” in *Proceedings of the Companion Conference on Genetic and Evolutionary Computation*, ser. GECCO ’23 Companion. New York, NY, USA: Association for Computing Machinery, 2023, p. 651–654.
- [11] Y. Tang, J. Sun, H. Wang, J. Deng, L. Tong, and W. Xu, “A method of network attack-defense game and collaborative defense decision-making based on hierarchical multi-agent reinforcement learning,” *Computers & Security*, vol. 142, p. 103871, 2024.
- [12] M. Kiely, D. Bowman, M. Standen, and C. Moir, “On autonomous agents in a cyber defence environment,” 2023, <https://arxiv.org/abs/2309.07388?context=cs>.
- [13] T. J. Richer and M. Standen, *Testing and Measurements*. Cham: Springer International Publishing, 2023, pp. 275–293. [Online]. Available: https://doi.org/10.1007/978-3-031-29269-9_13
- [14] B. Prebot, Y. Du, X. Xi, and C. Gonzalez, “Cognitive models of dynamic decisions in autonomous intelligent cyber defense,” 10 2022, 2nd International Conference on Autonomous Intelligent Cyber-Defense Agents, AICA 2022, Bordeaux, France, October 25–26, 2022.

TABLE 7: Defender interventions in CAGE-2 [4].

Type	Interventions	MITRE D3FEND TECHNIQUE
Monitor	Network monitoring Forensic analysis	D3-NTA network analysis D3-FA file analysis
Start decoys	APACHE, FEMITTER HARAKA, SMSS SSHD, SVCHOST, TOMCAT	D3-DE decoy environment D3-DE decoy environment D3-DE decoy environment
Restore	Restore node to a checkpoint Attempt to remove attacker	D3-RA restore access D3-FEV file eviction

[15] Y. Du, B. Prébot, X. Xi, and C. Gonzalez, "Towards autonomous cyber defense: Predictions from a cognitive model," *Proceedings of the Human Factors and Ergonomics Society Annual Meeting*, vol. 66, no. 1, pp. 1121–1125, 2022.

[16] A. Applebaum *et al.*, "Bridging automated to autonomous cyber defense: Foundational analysis of tabular q-learning," in *ACM Workshop on Artificial Intelligence and Security*, 2022. [Online]. Available: <https://doi.org/10.1145/3560830.3563732>

[17] J. Wiebe, R. A. Mallah, and L. Li, "Learning cyber defence tactics from scratch with multi-agent reinforcement learning," 2023.

[18] S. Xu, Z. Xie, C. Zhu, X. Wang, and L. Shi, "Enhancing cybersecurity in industrial control system with autonomous defense using normalized proximal policy optimization model," in *2023 IEEE 29th International Conference on Parallel and Distributed Systems (ICPADS)*, 2023, pp. 928–935.

[19] Y. Yan, Y. Zhang, and K. Huang, "Depending on yourself when you should: Mentoring ILM with RL agents to become the master in cybersecurity games," 2024, <https://arxiv.org/html/2403.17674v1>.

[20] Z. Cheng, X. Wu, J. Yu, S. Yang, G. Wang, and X. Xing, "Rice: Breaking through the training bottlenecks of reinforcement learning with explanation," 2024.

[21] J. F. Loevenich, E. Adler, R. Mercier, A. Velazquez, and R. R. F. Lopes, "Design of an autonomous cyber defence agent using hybrid AI models," in *2024 International Conference on Military Communication and Information Systems (ICMCIS)*, 2024, pp. 1–10.

[22] J. Pearl, *Causality: models, reasoning and inference*. Cambridge university press, 2009.

[23] K. Åström, "Optimal control of markov processes with incomplete state information," *Journal of Mathematical Analysis and Applications*, vol. 10, no. 1, pp. 174–205, 1965.

[24] D. Silver and J. Veness, "Monte-carlo planning in large pomdps," in *Advances in Neural Information Processing Systems*, vol. 23, 2010.

[25] CSLE, "Cyber security learning environment," 2023, documentation: <https://limmen.dev/csle/>, traces: <https://github.com/Limmen/csle/releases/tag/v0.4.0>, source code: <https://github.com/Limmen/csle>, video demonstration: <https://www.youtube.com/watch?v=iE2KPmtIs2A&>, installation: https://www.youtube.com/watch?v=l_g3sRJwwhc. [Online]. Available: <https://limmen.dev/csle/>

[26] B. Li, H. Wang, and G. Feng, "Adaptive hierarchical intrusion tolerant model based on autonomic computing," in *2008 International Conference on Security Technology*, 2008, pp. 137–141.

[27] J. Janisch, T. Pevný, and V. Lisý, "Nasimemu: Network attack simulator & emulator for training agents generalizing to novel scenarios," in *Computer Security. ESORICS 2023 International Workshops*. Springer Nature Switzerland, 2024, pp. 589–608.

[28] K. Hammar and R. Stadler, "Finding effective security strategies through reinforcement learning and Self-Play," in *International Conference on Network and Service Management (CNSM 2020)*, Izmir, Turkey, 2020.

[29] —, "Learning intrusion prevention policies through optimal stopping," in *International Conference on Network and Service Management (CNSM 2021)*, Izmir, Turkey, 2021, <https://arxiv.org/pdf/2106.07160.pdf>.

[30] —, "An online framework for adapting security policies in dynamic IT environments," in *18th International Conference on Network and Service Management (CNSM)*, 2022, pp. 359–363.

[31] —, "Intrusion prevention through optimal stopping," *IEEE Transactions on Network and Service Management*, vol. 19, no. 3, pp. 2333–2348, 2022.

[32] —, "Learning near-optimal intrusion responses against dynamic attackers," *IEEE Transactions on Network and Service Management*, vol. 21, no. 1, pp. 1158–1177, 2024.

[33] —, "Scalable learning of intrusion response through recursive decomposition," in *14th International Conference on Decision and Game Theory for Security*, 2023.

[34] T. Li, G. Peng, Q. Zhu, and T. Başar, "The confluence of networks, games, and learning a game-theoretic framework for multiagent decision making over networks," *IEEE Control Systems Magazine*, vol. 42, no. 4, pp. 35–67, 2022.

[35] T. Kunz, C. Fisher, J. L. Novara-Gsell, C. Nguyen, and L. Li, "A multiagent cyberbattlesim for RL cyber operation agents," 2023.

[36] K. Hammar, T. Li, R. Stadler, and Q. Zhu, "Automated security response through online learning with adaptive conjectures," 2024, <https://arxiv.org/abs/2402.12499>.

[37] K. Malialis and D. Kudenko, "Multiagent router throttling: Decentralized coordinated response against DDoS attacks," in *IAAI*, 2013.

[38] J. Nyberg and P. Johnson, "Training automated defense strategies using graph-based cyber attack simulations," 2023, workshop on SOC Operations and Construction (WOSOC) 2023.

[39] J. L. Hellerstein, Y. Diao, S. Parekh, and D. M. Tilbury, *Feedback Control of Computing Systems*. USA: Wiley & Sons, 2004.

[40] A. Teixeira, K. C. Sou, H. Sandberg, and K. H. Johansson, "Secure control systems: A quantitative risk management approach," *IEEE Control Systems Magazine*, vol. 35, no. 1, pp. 24–45, 2015.

[41] K. Hammar and R. Stadler, "Intrusion tolerance for networked systems through two-level feedback control," in *2024 54th Annual IEEE/IFIP International Conference on Dependable Systems and Networks (DSN)*, 2024, <https://arxiv.org/abs/2404.01741>.

[42] T. Li, K. Hammar, R. Stadler, and Q. Zhu, "Conjectural online learning with first-order beliefs in asymmetric information stochastic games," 2024, <https://arxiv.org/abs/2402.18781>.

[43] O. P. Kreidl and T. M. Frazier, "Feedback control applied to survivability: a host-based autonomic defense system," *IEEE Transactions on Reliability*, vol. 53, pp. 148–166, 2004.

[44] A. Teixeira, S. Amin, H. Sandberg, K. H. Johansson, and S. S. Sastry, "Cyber security analysis of state estimators in electric power systems," in *49th IEEE Conference on Decision and Control (CDC)*, 2010.

[45] L.-X. Yang, P. Li, X. Yang, Y. Xiang, F. Jiang, and W. Zhou, "Effective quarantine and recovery scheme against advanced persistent threat," *IEEE Transactions on Systems, Man, and Cybernetics: Systems*, vol. 51, no. 10, pp. 5977–5991, 2021.

[46] H. Zhang, P. Cheng, L. Shi, and J. Chen, "Optimal denial-of-service attack scheduling against linear quadratic gaussian control," in *2014 American Control Conference*, 2014, pp. 3996–4001.

[47] A. Andrew, S. Spillard, J. Collyer, and N. Dhir, "Developing optimal causal cyber-defence agents via cyber security simulation," in *Proceedings of the ML4Cyber workshop, ICML 2022, Baltimore, USA, July 17–23*. PMLR, 2022.

[48] K. Highnam, Z. Hanif, E. V. Vogt, S. Parbhoo, S. Maffeis, and N. R. Jennings, "Adaptive experimental design for intrusion data collection," in *CAMLIS'23: Conference on Applied Machine Learning for Information Security*, 2023, <https://arxiv.org/pdf/2310.13224>.

[49] D. Shi, Z. Guo, K. H. Johansson, and L. Shi, "Causality countermeasures for anomaly detection in cyber-physical systems," *IEEE Transactions on Automatic Control*, vol. 63, no. 2, pp. 386–401, 2018.

[50] W. G. Mueller, A. Memory, and K. Bartrem, "Causal discovery of cyber attack phases," in *2019 18th IEEE International Conference On Machine Learning And Applications (ICMLA)*, 2019, pp. 1348–1352.

[51] M. Tambe, *Security and Game Theory: Algorithms, Deployed Systems, Lessons Learned*, 1st ed. USA: Cambridge University Press, 2011.

[52] L. Buttyan and J.-P. Hubaux, *Security and Cooperation in Wireless Networks: Thwarting Malicious and Selfish Behavior in the Age of Ubiquitous Computing*. USA: Cambridge University Press, 2007.

[53] P. Lau, W. Wei, L. Wang, Z. Liu, and C.-W. Ten, "A cybersecurity insurance model for power system reliability considering optimal defense resource allocation," *IEEE Transactions on Smart Grid*, vol. 11, no. 5, pp. 4403–4414, 2020.

[54] S. Zonouz *et al.*, "Rre: A game-theoretic intrusion response and recovery engine," in *2009 IEEE/IFIP International Conference on Dependable Systems & Networks*, 2009.

[55] L. Huang and Q. Zhu, "A dynamic games approach to proactive defense strategies against advanced persistent threats in cyber-physical systems," *Computers & Security*, vol. 89, p. 101660, 11 2019.

[56] L. Zhang, T. Zhu, F. K. Hussain, D. Ye, and W. Zhou, "A game-theoretic method for defending against advanced persistent threats in cyber systems," *IEEE Transactions on Information Forensics and Security*, vol. 18, pp. 1349–1364, 2023.

[57] K. Horák, B. Bosanský, P. Tomásek, C. Kiekintveld, and C. A. Kamhoua, "Optimizing honeypot strategies against dynamic lateral movement using partially observable stochastic games," *Comput. Secur.*, vol. 87, 2019.

[58] O. Tsemogne, Y. Hayel, C. Kamhoua, and G. Deugoué, *Partially Observable Stochastic Games for Cyber Deception Against Network Epidemic*, 12 2020, pp. 312–325.

[59] K. C. Nguyen, T. Alpcan, and T. Basar, "Stochastic games for security in networks with interdependent nodes," in *2009 International Conference on Game Theory for Networks*, 2009, pp. 697–703.

[60] A. Aydeger, M. H. Manshaei, M. A. Rahman, and K. Akkaya, "Strategic defense against stealthy link flooding attacks: A signaling game approach," *IEEE Transactions on Network Science and Engineering*, vol. 8, no. 1, pp. 751–764, 2021.

[61] K. Wang, M. Du, S. Maharjan, and Y. Sun, "Strategic honeypot game model for distributed denial of service attacks in the smart grid," *IEEE Transactions on Smart Grid*, vol. 8, no. 5, pp. 2474–2482, 2017.

[62] A. Applebaum, S. Johnson, M. Limiero, and M. Smith, "Playbook oriented cyber response," in *2018 National Cyber Summit (NCS)*, 2018, pp. 8–15.

[63] M. Roesch, "Snort - lightweight intrusion detection for networks," in *Proceedings of the 13th USENIX Conference on System Administration*, ser. LISA '99. USA: USENIX Association, 1999, p. 229–238.

[64] Trellix, "Trellix intrusion prevention system," 2022. [Online]. Available: <https://www.trellix.com/en-us/products/intrusion-prevention-system.html>

[65] B. Foo, Y.-C. Mao, and E. Spafford, "Adepts: Adaptive intrusion response using attack graphs in an e-commerce environment," in *Proceedings of the 2005 International Conference on Dependable Systems and Networks*, ser. DSN '05, USA, 2005, p. 508–517.

[66] D. Yau, J. Lui, and F. Liang, "Defending against distributed denial-of-service attacks with max-min fair server-centric router throttles," in *IEEE 2002 Tenth IEEE International Workshop on Quality of Service (Cat. No.02EX564)*, 2002, pp. 35–44.

[67] M. Castro and B. Liskov, "Practical byzantine fault tolerance and proactive recovery," *ACM Trans. Comput. Syst.*, vol. 20, no. 4, p. 398–461, nov 2002. [Online]. Available: <https://doi.org/10.1145/571637.571640>

[68] M. Rigaki, O. Lukáš, C. A. Catania, and S. Garcia, "Out of the cage: How stochastic parrots win in cyber security environments," 2023, <https://arxiv.org/abs/2308.12086>.

[69] S. Moskal, S. Laney, E. Hemberg, and U.-M. O'Reilly, "Llms killed the script kiddie: How agents supported by large language models change the landscape of network threat testing," 2023, <https://arxiv.org/abs/2310.06936>.

[70] U.-M. O'Reilly and E. Hemberg, "An artificial coevolutionary framework for adversarial ai," in *AAAI Fall Symposium: ALEC*, 2018.

[71] S. Moskal, E. Hemberg, and U.-M. O'Reilly, "Cyberevo: evolutionary search of knowledge-based behaviors in a cyber attack campaign," in *Proceedings of the Genetic and Evolutionary Computation Conference Companion*, ser. GECCO '22. New York, NY, USA: Association for Computing Machinery, 2022, p. 2168–2176.

[72] R. Bronfman-Nadas, N. Zincir-Heywood, and J. T. Jacobs, "An artificial arms race: Could it improve mobile malware detectors?" in *2018 Network Traffic Measurement and Analysis Conference (TMA)*, 2018.

[73] B. Jia, Z. Lin, and Y. Ma, "Advanced persistent threat detection method research based on relevant algorithms to artificial immune system," in *Trustworthy Computing and Services*, L. Yueming, W. Xu, and Z. Xi, Eds. Berlin, Heidelberg: Springer Berlin Heidelberg, 2015, pp. 221–228.

[74] M. V. Shubhra Dwivedi and S. Tripathi, "Defense against distributed dos attack detection by using intelligent evolutionary algorithm," *International Journal of Computers and Applications*, vol. 44, no. 3, pp. 219–229, 2022. [Online]. Available: <https://doi.org/10.1080/1206212X.2020.1720951>

[75] F. F. De Vega, "A fault tolerant optimization algorithm based on evolutionary computation," in *2006 International Conference on Dependability of Computer Systems*, 2006, pp. 335–342.

[76] Y. Zhang, L. Wang, and Y. Xiang, "Power system reliability analysis with intrusion tolerance in scada systems," *IEEE Transactions on Smart Grid*, vol. 7, no. 2, pp. 669–683, 2016.

[77] H. Al-Hamadi and I.-R. Chen, "Redundancy management of multipath routing for intrusion tolerance in heterogeneous wireless sensor networks," *IEEE Transactions on Network and Service Management*, vol. 10, no. 2, pp. 189–203, 2013.

[78] X. Wang and R. Stadler, "It intrusion detection using statistical learning and testbed measurements," in *NOMS 2024-2024 IEEE/IFIP Network Operations and Management Symposium*, 2024, <https://arxiv.org/abs/2402.13081>.

[79] L. Huang and Q. Zhu, "Analysis and computation of adaptive defense strategies against advanced persistent threats for cyber-physical systems," in *Decision and Game Theory for Security*, L. Bushnell, R. Poovendran, and T. Başar, Eds. Cham: Springer International Publishing, 2018, pp. 205–226.

[80] H. Zhang, P. Cheng, L. Shi, and J. Chen, "Optimal denial-of-service attack scheduling with energy constraint," *IEEE Transactions on Automatic Control*, vol. 60, no. 11, pp. 3023–3028, 2015.

[81] J. Schulman, F. Wolski, P. Dhariwal, A. Radford, and O. Klimov, "Proximal policy optimization algorithms," *CoRR*, 2017, <http://arxiv.org/abs/1707.06347>. [Online]. Available: <http://arxiv.org/abs/1707.06347>

[82] W. Inc, "Wazuh - the open source security platform," 2022. [Online]. Available: <https://wazuh.com/>

[83] J. Zhang, D. Kumor, and E. Bareinboim, "Causal imitation learning with unobserved confounders," in *Proceedings of the 34th International Conference on Neural Information Processing Systems*, ser. NIPS '20, 2020.

[84] R. A. Fisher, *The Design of Experiments*. Edinburgh: Oliver and Boyd, 1935.

[85] I. Shpitser and J. Pearl, "Complete identification methods for the causal hierarchy," *Journal of Machine Learning Research*, vol. 9, no. 9, 2008.

[86] D. P. Bertsekas, *Dynamic Programming and Optimal Control*, 3rd ed. Belmont, MA, USA: Athena Scientific, 2005, vol. I.

[87] S. A. Murphy, "Optimal dynamic treatment regimes," *Journal of the Royal Statistical Society Series B*, vol. 65, no. 2, pp. 331–355, 2003.

[88] S. Lee and E. Bareinboim, "Structural causal bandits with non-manipulable variables," in *Proceedings of the AAAI Conference on Artificial Intelligence*, vol. 33, 2019, pp. 4164–4172.

[89] H. W. Kuhn, *Extensive games and the problem of information*. Princeton, NJ: Princeton University Press, 1953.

[90] J. Peters, D. Janzing, and B. Schlkopf, *Elements of Causal Inference: Foundations and Learning Algorithms*. The MIT Press, 2017.

[91] W. L. Buntine, "Operations for learning with graphical models," *J. Artif. Int. Res.*, vol. 2, no. 1, p. 159–225, dec 1994. [Online]. Available: <https://doi.org/10.1613/jair.62>

[92] C. T. Ionescu Tulcea, "Mesures dans les espaces produits," *Lincei-Rend. Sc. fis. mat. e nat.*, vol. 7, pp. 208–211, 1949.

[93] V. Krishnamurthy, *Partially Observed Markov Decision Processes: From Filtering to Controlled Sensing*. Cambridge University Press, 2016.

[94] I. Shpitser and J. Pearl, "Identification of conditional interventional distributions," in *Proceedings of the Twenty-Second Conference on Uncertainty in Artificial Intelligence*, ser. UAI'06. Arlington, Virginia, USA: AUAI Press, 2006, p. 437–444.

[95] S. Thrun, W. Burgard, and D. Fox, *Probabilistic robotics*. Cambridge, Mass.: MIT Press, 2005.

[96] D. Crisan and A. Doucet, "A survey of convergence results on particle filtering methods for practitioners," *IEEE Transactions on Signal Processing*, vol. 50, no. 3, pp. 736–746, 2002.

[97] C. H. Papadimitriou and J. N. Tsitsiklis, "The complexity of markov decision processes," *Math. Oper. Res.*, vol. 12, p. 441–450, Aug. 1987.

[98] L. Kocsis and C. Szepesvári, "Bandit based monte-carlo planning," in *ECML*, ser. Lecture Notes in Computer Science, J. Fürnkranz, T. Scheffer, and M. Spiliopoulou, Eds., vol. 4212. Springer, 2006, pp. 282–293.

[99] T. Lattimore and C. Szepesvári, *Bandit algorithms*. Cambridge University Press, 2020.

[100] M. Wolk, A. Applebaum, C. Dennler, P. Dwyer, M. Moskowitz, H. Nguyen, N. Nichols, N. Park, P. Rachwalski, F. Rau, and A. Webster, "Beyond cage: Investigating generalization of learned autonomous network defense policies," 2022.

[101] E. Çınlar, *Probability and Stochastics*, ser. Graduate Texts in Mathematics. Springer New York, 2011.

[102] J. S. Rosenthal, *A first look at rigorous probability theory*, 2nd ed. World Scientific Publishing Co. Pte. Ltd., Hackensack, NJ, 2006.

[103] P. Auer, N. Cesa-Bianchi, and P. Fischer, "Finite-time analysis of the multiarmed bandit problem," *Machine Learning*, vol. 47, no. 2, pp. 235–256, May 2002. [Online]. Available: <https://doi.org/10.1023/A:1013689704352>

[104] T. Dam, P. Klink, C. D'Eramo, J. Peters, and J. Pajarinen, "Generalized mean estimation in monte-carlo tree search," in *Proceedings of the Twenty-Ninth International Joint Conference on Artificial Intelligence*, ser. IJCAI'20, 2021.

[105] M. Standen, M. Lucas, D. Bowman, T. J. Richer, J. Kim, and D. Marriott, "Cyborg: A gym for the development of autonomous cyber agents," *CoRR*, 2021, <https://arxiv.org/abs/2108.09118>.

[106] T. M. Corporation, "Cve database," 2022, <https://cve.mitre.org/>. [Online]. Available: <https://cve.mitre.org/>

[107] ———, "Cwe list," 2023, <https://cwe.mitre.org/index.html>. [Online]. Available: <https://cwe.mitre.org/index.html>